POLYPUBLIE
Polytechnique Montréal

POLYTECHNIQUE MONTRÉAL
UNIVERSITÉ D'INGÉNIERIE

Titre: Title:	Coupled non-conforming finite element and finite difference approximation based on laminate extrapolation to simulate liquid composite molding processes. Part II: non-isothermal Filling and Curing
Auteurs: Authors:	Edu Ruiz, & François Trochu
Date:	2007
Type:	Article de revue / Article
Référence: Citation:	Ruiz, E., & Trochu, F. (2007). Coupled non-conforming finite element and finite difference approximation based on laminate extrapolation to simulate liquid composite molding processes. Part II: non-isothermal Filling and Curing. Science and Engineering of Composite Materials, 14(2), 113-144. https://doi.org/10.1515/secm.2007.14.2.113

Document en libre accès dans PolyPublie
Open Access document in PolyPublie

URL de PolyPublie: PolyPublie URL:	https://publications.polymtl.ca/21442/
Version:	Version officielle de l'éditeur / Published version Révisé par les pairs / Refereed
Conditions d'utilisation: Terms of Use:	CC BY-NC-ND

Document publié chez l'éditeur officiel
Document issued by the official publisher

Titre de la revue: Journal Title:	Science and Engineering of Composite Materials (vol. 14, no. 2)
Maison d'édition: Publisher:	de Gruyter
URL officiel: Official URL:	https://doi.org/10.1515/secm.2007.14.2.113
Mention légale: Legal notice:	©2011 by Walter de Gruyter GmbH & Co. This article is distributed under the terms of the Creative Commons Attribution Non-Commercial License, which permits unrestricted non-commercial use, distribution, and reproduction in any medium, provided the original work is properly cited.

Ce fichier a été téléchargé à partir de PolyPublie, le dépôt institutionnel de Polytechnique Montréal
This file has been downloaded from PolyPublie, the institutional repository of Polytechnique Montréal

https://publications.polymtl.ca

Coupled Non-Conforming Finite Element and Finite Difference Approximation Based on Laminate Extrapolation to Simulate Liquid Composite Molding Processes. Part II: Non-Isothermal Filling and Curing

Edu Ruiz* and F. Trochu

Centre de Recherches Appliquées Sur les Polymères (CRASP), Département de Génie Mécanique, École Polytechnique de l'Universite de Montréal, H3C 3A7, Canada

ABSTRACT

A numerical methodology is presented for the accurate simulation of non-isothermal mold filling in Liquid Composite Molding. Starting with a mid-surface mesh and based on the structure of the fabric reinforcement, the extrapolation algorithm described in /17/ is used to generate 3D finite elements or parallel layers of 2D elements. To solve the coupled flow/energy/chemical species equations, two methodologies are used. The finite element formulation presented in /17/ is first coupled with a 3D finite element formulation for heat and curing analyses. In the second approach, a hybrid finite element and finite difference model is proposed. As the heat conduction and convection is evaluated in the plane of the elements by the finite element formulation, the through-thickness heat flow is computed by a one-dimensional finite difference approximation. The combination of the three-dimensional mesh extrapolated in parallel layers with the thermal formulations allows investigating diverse degrees of coupling between the fluid and heat flows. With the same initial 2D mesh and material data, the user can easily define the level of complexity to be used in the numerical model. The results of the thermal formulations are validated with analytical tests. The performance of the model as well as the gain in cpu time are summarized. Finally a test case is presented to illustrate the advantages of the coupled model in terms of accuracy

Key Words: Liquid Composite Molding (LCM), composites processing modeling, non-conforming finite element, non-isothermal simulation, mesh extrapolation.

INTRODUCTION

Liquid Composite Molding (LCM) refers to a group of related and widely used manufacturing processes for composite materials. These processes consist in general of injecting a thermosetting resin in a closed mold where a dry-fibrous reinforcement has been placed. During the process, a catalyzed resin is injected under pressure into the pre-heated mold cavity. In case of thermosets, the resin reacts and solidifies during the curing phase. Once the resin has cured, the mold is opened and the composite part is demolded. The flow front locations in time, the pressure distribution and the temperature field are the main parameters that govern the molding process and the final properties of the part. These parameters can be predicted by numerical simulations during the filling and curing stages, to assist in designing the mold and improve the manufacturing

* e-mail: edu.ruiz@polymtl.ca
Postal address: C.P. 6079, succ. Centre-Ville
Montreal (Quebec) Canada, H3C 3A7
Tel.: Edu Ruiz: (514) 340-4711 ext. 4585; Fax: (514) 340-5867
Fax Number: (514) 340-5867

process. During last decade, several computational studies have demonstrated that modeling and process simulation can help in tool design by providing preliminary information of fluid and heat flow evolutions. However, due to the complexity of the physical phenomena involved in LCM and their intrinsic coupling, a series of non-linear differential equations must be solved iteratively. For large scale models, a significant computational effort is required to run a complete simulation of the manufacturing process. This renders the optimization of the full process a complex numerical challenge.

The control of heat transfer and chemical reaction in LCM is complex because a hard number of factors interact. As schematically indicated in Figure 1, four categories of phenomena occur during composite processing: rheological, thermal, chemical and viscoelastic. The resin flowing across the mold cavity absorbs heat by conduction from the mold walls and from the heated preform; temperature is also transported by convective forces. The rheological phenomena depend on the temperature and degree of conversion of the resin via the resin viscosity. In turn, the velocity field characterizing the fluid flow transports the chemical species and influences the thermal field. It also determines how the mold is going to be filled up by the resin and the quantity of heat that will be generated by viscous dissipation. On one hand, the chemical reactivity of the resin increases with temperature, on the other hand the exothermy of the polymerization reaction is usually sufficient to increase the temperature notably. Resin thermal and mechanical properties such as specific heat, thermal conductivity or elastic modulus depend on temperature and resin degree of conversion. The strain-stress relationship depends on temperature through the thermal expansion/contraction of the resin; it is also related to the degree of cure via the chemical shrinkage produced during the cross-linking polymerization. Finally, viscoelastic behaviour of the polymer depends on temperature, degree of cure and time (stress relaxation is observed during cure). The multiple interactions between these phenomena make the numerical modeling of the full process a complex, and sometimes unfeasible, task.

Researchers have resolved this complexity by building mathematical models of flow, heat transfer, chemical reaction and strain-stress relationship. Finite element software has been developed to implement some of these mathematical models for complex three-dimensional parts /1-10/. The energy equation was solved both by finite element and finite difference. Guyonvarch *et al.* /1/ presented a heat transfer analysis integrated with a non-isothermal 3D filling model. They used a Taylor-Galerkin method in a finite element model that guarantees a reasonable stability and accuracy of the temperature calculation even when convection becomes dominant. However, the scheme is not unconditionally stable, which creates numerical difficulties.

Lebrun *et al.* /2/ conducted an experimental investigation of heat transfer during the filling stage by measuring temperatures through the thickness of the part at four different locations in the flow direction. The authors presented a finite difference program used to calculate the temperature distribution through the thickness of the steel wall. Finally, the authors presented a model for the Nusselt number, which takes into account the effects of thermal dispersion, variable resin viscosity, fiber volume content and mold temperature.

In order to incorporate these considerations in non-isothermal filling simulations, Audet /18/ implemented a Taylor-Galerkin method to solve the energy equation. Even if Taylor series approximation leads to both explicit and implicit numerical scheme, for stability considerations the implicit one was used. To minimize the numerical oscillations that tend to perturb the temperature distribution in transport problems coupled with diffusion, a second order Taylor series was considered. Although numerical stability is guaranteed, when convective terms become dominant in the heat flow, temperature oscillations appear at the boundaries. In extension of the model of Audet, Bohr /3/ used a standard Galerkin formulation with an artificial diffusion term. In this approach, the thermal instabilities of the numerical scheme were solved by coupling the Galerkin formulation with the piecewise discontinuous finite element approximation of Lesaint-Raviart for transport problems. The resulting coupled formulation with a time Gear interpolation for the transient solution is unconditionally stable and does not require smaller

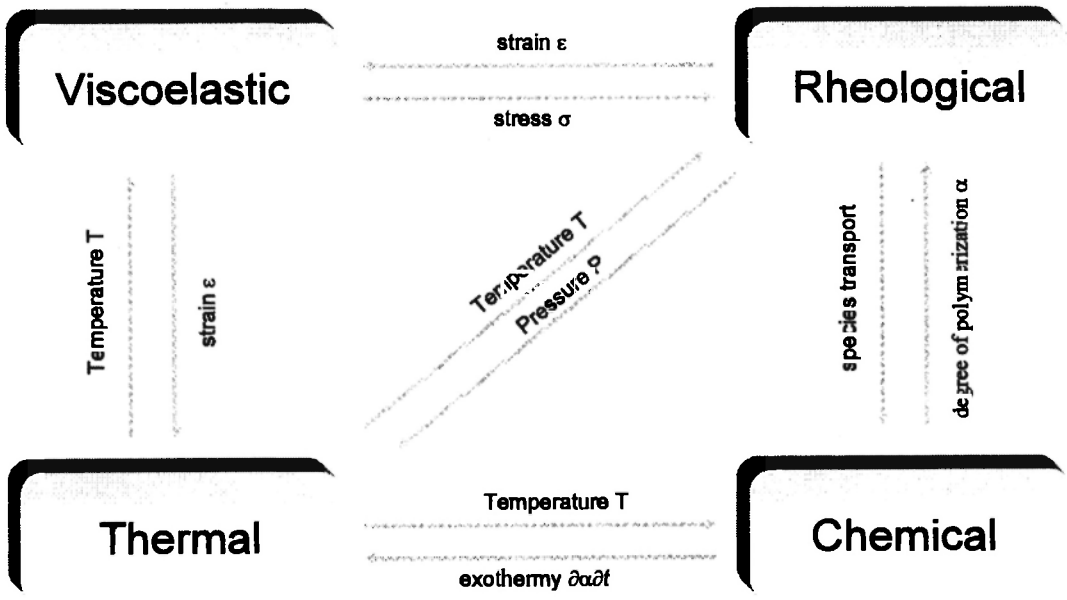

Fig. 1: Coupling of physical phenomena in Liquid Composite Molding (LCM).

time step iterations.

Tucker /4/ presented a comprehensive analysis of the issues in the modeling of heat transfer and chemical reaction in resin transfer molding and structural reaction injection molding. A rigorous derivation of the governing equations by the local volume averaging method has cleared up ambiguities about how some terms should be handled, and has clearly shown the need of adding dispersion terms in the energy balance and cure equations. The author has also introduced a useful set of dimensionless parameters for the flow, heat transfer and cure models, and provides analytical solutions in some specific cases.

Gauvin and Trochu /5/ analyzed non-isothermal fluid flows through multilayer preforms. Experimental results showed the influence of the mold temperature on the distribution of the resin temperature through the thickness of a composite. Since resin viscosity is highly sensitive to temperature, they suggested that a reliable simulation should take this dependence into account. Although the three-dimensional solution of the filling stage is robust and accurate, it still requires a large amount of computational time. Since the thickness of the cavity is usually small compared to the characteristic length of the part, it defines the size of the mesh used in numerical simulations. A minimum number of finite elements through the thickness of the part is necessary in order to obtain an acceptable solution. Moreover, the aspect ratio of these elements can not be too small to avoid numerical inconsistencies. These limitations result in a very dense mesh, which makes the three-dimensional finite element implementation of the solver highly computer intensive. The large number of degrees of freedom needed to model complex three-dimensional composite parts results in time consuming calculations that makes process optimization extremely difficult, if not impossible.

Extensive efforts have been made by researchers to decrease the computer time required to solve the coupled flow and thermal formulations. In a thin mold cavity, the flow may be simplified to a two-dimensional problem, but the three-dimensional heat transfer problem must be considered as such because of the important heat convection in the planar direction and heat conduction through the thickness of the part. When LCM parts are considered as thin shells, the

permeability, diffusion and dispersion tensors are homogeneous through the thickness. In addition, thermal and chemical species diffusion due to mechanical dispersion is assumed to be of purely kinematic origin, and thus proportional to the velocity norm. Since the velocity can be neglected in the thickness direction, the chemical species dispersion may be evaluated in the planar direction only, so that two-dimensional flow analysis can be carried out with three-dimensional heat transfer calculations.

To solve this simplified problem, different approximations have been suggested. Bruschke and Advani /8/ proposed a mixed model based on in-plane flow solution (by 2D finite elements and element control volume) while the heat conduction/convection is solved by finite differences (FD) in 3D. The through-thickness heat convection is neglected and only in-plane heat transport is introduced into the FD thermal formulation. The convection term is added to the FD model using a thickness averaged velocity. In a similar way, Ngo and Tamma /9/ have used a 2D FE formulation for the in-plane flow and a 3D FE formulation for the heat conduction/convection. The fluid flow calculation was based on the nodal control volume approach with conforming finite element approximation. To improve the numerical stability of the thermal formulation, the Streamline Upwind Petrov-Galerkin (SUPG) weighting functions were employed. The algorithm presented accounts for the three-dimensional mesh generation used to solve the heat transport problem and sub-time stepping of the filling time step to ensure the stability of the thermal solution. These methods are faster than full three-dimensional analysis but only consider a thickness-averaged permeability and resin viscosity. In fact, an averaged flow front is calculated in the midplane of the mold cavity. Moreover, finite difference formulations are not unconditionally stable when implemented to solve heat conduction and convection problems. For accurate solutions, the FD grid or the time step must be refined as a function of Fourier's and Nusselt's numbers. In practice, when the heat flow is dominated by convection, which is usually the case in Resin Transfer Molding (RTM), the number of time steps required to properly solve the FD model for each iteration of the flow solution turns out to make the calculations very computer intensive.

Based on physical considerations and on the combined implementation of several numerical algorithms, a new methodology is proposed to solve the non-isothermal filling and curing phases in LCM. It consists of combining different FE and FD formulations depending on the degree of coupling needed between the thermal and flow phenomena to simulate accurately the manufacturing process. Starting with a midplane mesh, different options are possible. In the simplest case, no significant coupling is assumed to exist between the fluid flow and the heat transfer in the through-thickness direction. A numerical in-plane solution of the two-dimensional fluid flow and heat transfer is sufficient if it is coupled with a one-dimensional heat transfer analysis. When a full coupling has to be considered, a pure three-dimensional flow and thermal analysis can be carried out. Between these two solutions, various levels of coupling can be implemented on the same 2D mesh. The proposed algorithm permits the user to specify the level of complexity of the analysis without any additional meshing effort. A series of tests are carried out to validate by comparison with analytical results the different models proposed. Finally, a typical part will be analyzed to demonstrate the capabilities of the numerical algorithms implemented in this investigation.

GOVERNING EQUATIONS

Momentum equation

In the past /17/, a system of non-linear partial differential equations has been formulated in order to evaluate the flow of Newtonian fluids through a porous medium. The model accounts for isothermal flows in undeformable media and considers pressure of flow rate boundary conditions. In this part of the work, non-isothermal viscous flows in porous media will be modelled in presence of heat sources. The equation of mass conservation for the fluid phase can be written as:

$$div(\rho_f . \vec{v}) = 0 \qquad (1)$$

where ρ_r is the density of the injected resin and $\bar{v}$ is the superficial fluid velocity. Darcy's law for Newtonian fluid flow through porous media was used as momentum equation and is expressed as follows:

$$\bar{v} = -\frac{1}{\mu}[K].\nabla p \tag{2}$$

in which $[K]$ is the permeability tensor, taking the form of a 3x3 matrix, μ is the resin viscosity and ∇p the pressure gradient. Polymer viscosity depends on temperature and on chemical changes during polymerization. The rheological characterization of reactive materials is complex because of the large number of variables that come into play. Polymer rheology is influenced by the chemical formulation and filler concentration (in general calcium carbonate). The viscosity of a reactive resin system is a function of pressure, temperature, shear rate and time. The time dependence is due to the growing size of the polymer molecules as polymerization progresses. Therefore, viscosity can be defined as:

$$\mu = f(P, T, \dot{\gamma}, \alpha, \varphi) \tag{3}$$

where T, $\dot{\gamma}$, α and φ denote respectively temperature, shear rate, resin degree of cure and filler concentration. In LCM, the reactive system is injected at low viscosity. Viscosity increases with conversion and reaches an infinite value when the material solidifies either by chemical cross-linking or as result of physical changes such as phase separation or crystallization. During processing, mold filling must be completed before resin viscosity reaches a too high value. The upward limit of resin viscosity is attained at the gel point. As demonstrated by Han and Lem /11/, non-Newtonian effects appear to be small for polymer built up from breached monomers, except near the gel point. Most viscosity models for reactive resins neglect the non-Newtonian effects because temperature and network formation tend to dominate the rheological changes.

Although it is usually valid to consider flow and cure independently, high speed processing may imply that some conversion occurs during resin impregnation. Conversion-based viscosity models have been extensively applied to polymers. The most widely used rheological model that accounts for the effect of polymer conversion on viscosity is the Castro-Macosko model /12/:

$$\mu(T,\alpha) = \mu(T) \cdot \left(\frac{\alpha_{gel}}{\alpha_{gel} - \alpha} \right)^{C_1 + C_2 \cdot \alpha} \tag{4}$$

$$\mu(T) = C_T \cdot \exp\left(\frac{T_g}{T} \right) \tag{5}$$

where α and α_{gel} are the instantaneous and gelation chemical conversions respectively, C_1, C_2, and C_T are empirical constants, and T_g is the polymer glass transition temperature.

Energy and chemical species

In order to model the influence of heat transfer on the temperature of the resin, mold and fibrous reinforcement, it is necessary to carry out an energy balance between each of the constituents. In general, two approaches may be followed to find the temperature field /13-15/. In the first one, the resin and the fibers are considered as separate constituents (two phase model) used their temperatures may differ at any point of the mold. In the second approach, the resin and fibers are assumed to be at the same temperature (the so-called *lumped* system). In general, the equilibrium model, i.e. the second approach, is considered reasonably accurate for RTM /13, 15/, in which fluid flow is relatively slow. Considering the lumped system, the energy and chemical species balance equations for the resin-fiber mix leads to a transient temperature T solution of the following equation:

$$\tilde{\rho}\ \tilde{C}p \frac{\partial T}{\partial t} + \phi \rho_r\ Cp_r \nabla(\bar{v} \cdot T) + \nabla(\bar{v} \cdot p) = \left\{ \nabla([\tilde{k}] + [k_D])\ \nabla T \right\} + \phi \rho_r H_{Tot} \dot{H} \tag{6}$$

where the density $\tilde{\rho}$, heat capacity $\tilde{C}p$ and conductivity $\tilde{k}$ of the composite are the effective properties defined as:

a for non-impregnated fibers

$$\tilde{C}p = Cp_a w_a + Cp_f w_f \ ,$$

$$\tilde{\rho} = (\rho_a \rho_f)/(\rho_a w_a + \rho_f w_f)$$

$$\tilde{k} = (k_a k_f)/(k_a w_a + \bar{k}_f w_f),$$
$$w_a = (\phi/\rho_f)/(\phi/\rho_f + (1-\phi/\rho_a)) \quad (7a)$$
$$w_f = 1 - w_a$$

b for impregnated fibers

$$\tilde{C}p = Cp_r w_r + Cp_f w_f,$$
$$\tilde{\rho} = (\rho_r \rho_f)/(\rho_r w_r + \rho_f w_f)$$
$$\tilde{k} = (k_r k_f)/(k_r w_r + \bar{k}_f w_f),$$
$$w_r = (\phi/\rho_f)/(\phi/\rho_f + (1-\phi/\rho_r)) \quad (7b)$$
$$w_f = 1 - w_r$$

In the above equations ϕ is the porosity and w_r, w_f and w_a denote the weight fractions of resin fibers and air, respectively. Note that the conductivity tensor $[\tilde{k}]$ of the composite is averaged in each direction. The subscript r stands for the resin, f for the fibers and a for the air. The coefficient $[k_D]$ represents the thermal dispersion tensor arising from hydrodynamic dispersion. It can be evaluated as a function of Peclet number or characterized experimentally as a function of the fluid velocity /2, 18/.

The following initial and boundary conditions are required to solve the energy equation (6):

$T = T_r^{inj}$ at the injection gates

$T = T_f$ or $q = (1-\phi)\rho_f Cp_f (\hat{n}\cdot\bar{v})(T_f - T)$

at the flow front

$q = h_{eff} A \cdot (T_{wall} - T)$ at mold walls

where T_r^{inj} and T_f denote the resin temperature at the injection gate and the temperature of the dry fibrous reinforcement, respectively, T_{wall} is the mold temperature at the surface (i.e. at the interface between mold and the fluid flow), h_{eff} denotes the effective heat transfer coefficient between the mold wall and the fluid, and q represents the heat flow through the surface area A.

The source term on the right side of equation (6) accounts for the internal heat generated by the exothermic chemical reaction in thermoset resin systems. The value $H_{Tot}\dot{H}$ denotes the instantaneous heat generated by the cross-linking polymerization reaction and H_{Tot} is the total or ultimate heat of reaction during cure. This source term is usually assumed to be proportional to the reaction rate $d\alpha/dt$.

Conservation of chemical species can be expressed through the continuity equation:

$$\phi \frac{\partial \alpha}{\partial t} + \bar{v}\cdot\nabla\alpha = \phi \dot{H} \quad (9)$$

To compute the energy equation (6), the dependence of the reaction rate must be modeled as a function of temperature and degree of polymerization α. The empirical autocatalytic model of Kamal-Sourour /16/ that describes free-radical polymerization reaction is used in this study and can be formulated as follows:

$$\frac{d\alpha}{dt} = \left(A_1 \cdot \exp\left(\frac{-E_1}{R\cdot T}\right) + A_2 \cdot \exp\left(\frac{-E_2}{R\cdot T}\right)\cdot \alpha^{m_1} \right)\cdot (1-\alpha)^{n_1} \quad (10)$$

where coefficients A_1 and A_2 are Arrhenius constants, E_1 and E_2 are activation energies, R is the ideal gas constant and, n_1 and m_1 are the catalytic constants.

FINITE ELEMENTS FORMULATION

Following the procedure described in /17/ for the flow model, the energy balance equation (6) can be integrated over a control volume as:

$$\frac{\partial}{\partial t}\int_\Omega \tilde{\rho}\tilde{C}p\, T\, d\Omega + \int_\Gamma \rho_r Cp_r \cdot (\hat{n}\cdot\bar{v})\nabla T\, d\Gamma + \int_\Gamma (\hat{n}\cdot\bar{v})\nabla P\, d\Gamma$$
$$- \int_\Gamma \nabla(\hat{n}\cdot([\tilde{k}]+[K_D])\nabla T)\, d\Gamma = \int_\Omega \phi\rho_r H_{Tot}\dot{H}\, d\Omega \quad (12)$$

where Ω is the integration domain (in this case the volume of the element). The numerical solution of the integral energy equation is based on the standard Galerkin implemented by Bohr /3/. A Lesaint-Raviart formulation that avoids artificial oscillations is used to solve the transport problem. This method is based on the

separation of the coupled convection/diffusion problem into a convective and a diffusive solution. The heat diffusion is initially solved by a standard Galerkin formulation; then temperature is transported using the Lesaint-Raviart approximation with discontinuous finite elements. In the presence of thermal convection, the transport equation can be written in the following form:

$$\frac{\partial T}{\partial t} + \bar{v} \cdot \nabla T = f \ , \ \text{on} \ \Omega \qquad (13)$$
$$T = T(t) \ , \ \text{on} \ \Gamma_q$$

where T is the temperature transported at velocity $\bar{v}$ on the domain Ω, and $T(t)$ is an imposed temperature at the domain boundary Γ_q (usually the resin injection temperature). Note that the same nomenclature already defined in *Part I* of this work applies to the domain Ω and boundaries Γ_q and Γ_d. Function f represents a source term that can be a function of time and position. Using a variational formulation, the weak form of equation (13) is expressed as:

$$\int_\Omega w \left(\frac{\partial T}{\partial t} + \bar{v} \cdot \nabla T \right) d\Omega = \int_\Omega w f \, d\Omega + \int_{\Gamma_d} \left| T^+ - T^- \right| (\hat{n} \cdot \bar{v}) \, d\Gamma_d \qquad (14)$$

for a test function w belonging to the space $F(\Omega)$, where T^+ and T^- are the temperature values on the two sides of the boundary Γ_d. The finite element solution of equation (14) is an iterative process that consists of building a sequence of elements in the fluid flow domain. Beginning with the elements adjacent to the injection gate, the temperature is transferred using an upwind scheme based on to the mesh connectivity. The heat convection is finally solved using a Gear implicit scheme for the time derivative:

$$\int_\Omega w \left(\frac{1.5T^n - 2T^{n-1} + 0.5T^{n-2}}{\Delta t} + \bar{v} \cdot \nabla T^n \right) d\Omega = \int_\Omega w f \, d\Omega + \int_{\Gamma_d} \left| T^{n+} - T^{n-} \right| (\hat{n} \cdot \bar{v}) \, d\Gamma_d \qquad (15)$$

where indices n, n-1 and n-2 account for the actual and previous time steps. To evaluate the temperature field, a classical predictor-corrector method is used. The temperature is predicted by the diffusion equation and corrected by the convection solution. The iterative procedure consists of advancing half a time step in conduction and the other half in convection. The approximation of the energy equation by a sequence of conductive and convective solutions requires the continuity of the scalar field (i.e. the temperature field) at the nodes of the Galerkin formulation. For this reason, conforming shape functions are used in the 2D and 3D finite element approximations of the conduction/diffusion equation (6).

In a similar way to the energy equation, the balance of chemical species is solved separately for convection and for the polymerization reaction. The convective term of equation (9) can then be written as follows:

$$\int_\Omega w \left(\frac{\partial \alpha}{\partial t} + \bar{v} \cdot \nabla \alpha \right) d\Omega = \int_{\Gamma_d} \left| \alpha^+ - \alpha^- \right| (\hat{n} \cdot \bar{v}) \, d\Gamma_d \qquad (16)$$
$$\alpha = \alpha_0 \ , \ \text{on} \ \Gamma_q$$

where α_0 is the initial degree of cure at the boundary Γ_q (generally the injection gate). The diffusion of chemical species is governed by a partial differential equation that requires proper time integration. Bohr /3/ proposed to use fourth and fifth orders Runge-Kutta methods to solve the differential equation (10) of resin polymerization. In this paper, the fourth order Runge-Kutta method is used to evaluate the polymerization reaction. The degree of cure obtained is then transported with the Lesaint-Raviart integral formulation (16).

SOLUTION OF SHELL-LIKE GEOMETRIES

Finite element analysis is widely recognized as an accurate approximation method to solve coupled flow and thermal problems. One of the main advantages of this technique lies in its ability to minimize the temperature oscillations induced by convection terms. Even if complex solutions of non-isothermal flows are unconditionally stable, one main disadvantage is the computational cost. In three-dimensional modeling, the large number of elements required for proper spatial

discretization leads to time consuming simulations. In many cases, a compromise has to be sought between accuracy and computer time. Since in LCM applications the thickness is usually much smaller than the other dimensions of the part, a very large number elements is required to model through-thickness variations of permeability or of viscosity in the case of non-isothermal injections. As a result the resin flows with a different velocity in each layer of the composite. If these velocity changes are important, a three-dimensional analysis becomes unavoidable.

Note that a non-uniform viscosity appears through the thickness of a composite shell when the mold walls are heated at a higher temperature than the fibers and the resin injected (see Figure 2). The temperature dependence of viscosity will induce velocity variations and a through-thickness resin flow. When a gap-wise averaged velocity is acceptable, the flow equation (2) can be reduced to the following two-dimensional form:

$$\begin{bmatrix} v_\xi \\ v_\gamma \end{bmatrix} = -\begin{bmatrix} S_{\xi\xi} & S_{\xi\gamma} \\ S_{\gamma\xi} & S_{\gamma\gamma} \end{bmatrix} \cdot \begin{bmatrix} \dfrac{\partial P}{\partial \xi} \\ \dfrac{\partial P}{\partial \gamma} \end{bmatrix} \tag{17}$$

$$\begin{bmatrix} S_{\xi\xi} & S_{\xi\gamma} \\ S_{\gamma\xi} & S_{\gamma\gamma} \end{bmatrix} = \frac{1}{h_\tau} \int_{-\frac{h_\tau}{2}}^{\frac{h_\tau}{2}} \frac{1}{\mu(\xi,\gamma,\tau,T,\alpha)} \cdot \begin{bmatrix} K_{\xi\xi} & K_{\xi\gamma} \\ K_{\gamma\xi} & K_{\gamma\gamma} \end{bmatrix} \cdot d\tau$$

where ξ and γ are the local coordinates of the planar geometry, τ denotes the gapwise coordinate and h_τ is the thickness of the gap. The velocity components v_ξ and v_γ are the gapwise averaged values in the planar directions, and $[K]$ is the in-plane permeability tensor.

The mold walls in LCM have a strong influence on the energy balance. This implies that the heat transfer must be analyzed not only in the cavity but also in the mold. When three-dimensional FE formulations are used, the disperse matrix requires a large cpu time to be solved. If pure 3D finite differences (FD) solutions are implemented, undesirable temperature oscillations appear in convection dominated flows. In this work, a hybrid scheme is proposed to evaluate the three-dimensional energy equation, so as to obtain a stable and efficient numerical methodology to calculate non-isothermal flows and curing phases in shell composite parts. Based on the concept of separation of the conduction and convection phenomena, the approach consists of solving the 3D heat conduction by coupling the two-dimensional in-plane solution of the convective heat transfer with a one-dimensional through-thickness heat conduction analysis. First, the in-plane thermal conduction is calculated by the standard Galerkin formulation. Then, with the gapwise averaged velocity the planar convection is computed by the Lesaint-Raviart transport approximation. Once temperature is corrected, the through-thickness conduction and curing are evaluated by a finite difference approximation. Using successive half time stepping, the three formulations are solved for a single flow time step. Note that in this procedure, the connectivity of the finite

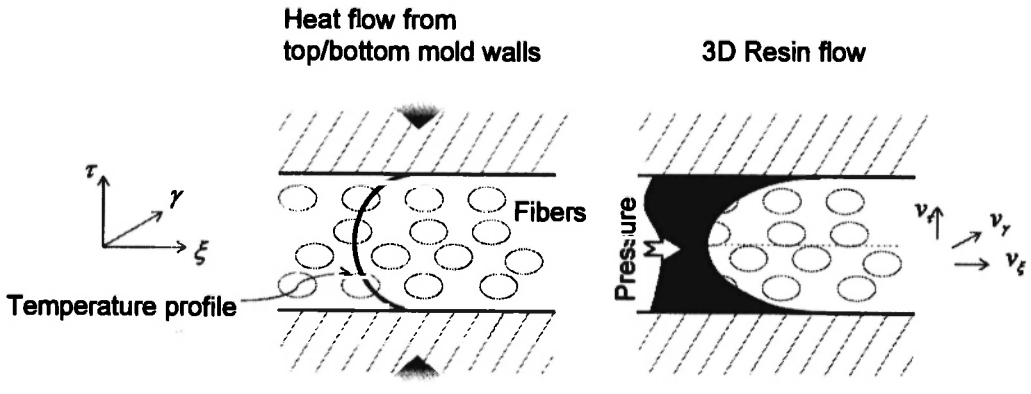

Fig. 2: Cross-section of the mold cavity showing the three-dimensional heat and fluid flows. The trough-thickness temperature profile results in variable resin viscosity and transverse fluid flow.

element mesh exists only in the two-dimensional space while finite difference nodes are coupled only in the thickness direction. The matrices of the FD formulation are tridiagonal (or quasi tridiagonal), so the numerical solution is highly efficient in terms of computer time. The stability of this numerical scheme is guaranteed because each of the formulations is unconditionally stable. In addition, any temperature oscillation induced by the FD approximation is diffused during the same time step by the FE solution.

FINITE DIFFERENCE FORMULATION

The solution of the through-thickness energy balance involves a subdivision of the in-plane control volumes (defined by the finite element edges) into a certain number of layers. The Galerkin finite element approximation of the heat conduction problem is calculated with conforming shape functions. This implies that the temperature scalar field is evaluated at the element nodes. In the hybrid FE/FD scheme, the connection between two-dimensional FE and one-dimensional FD formulations must then be done through the element nodes. As depicted in Figure 3, the finite difference nodes are extrapolated from the mesh nodes by the extrapolation algorithm described in /17/. Every FD node is associated to a control volume bound by the centroids and the mid-edges of the connected elements. The energy balance equation (6) becomes Fourier's heat conduction equation in one dimension. The volume averaged 1D Fourier's equation is written as:

$$V\ \tilde{\rho}\ \tilde{C}p\ \frac{\partial T}{\partial t} = A\ \tilde{k}_{\tau}\ \frac{\partial^2 T}{\partial \tau^2} + V\ \phi\ \rho_r H_{Tol}\dot{H} \tag{18}$$

where $T(t,\tau)$ is the transient absolute temperature at position τ through the total part thickness *part_thickness* ($0 < \tau \leq$ *part_thickness*), A and V denote respectiveiy the interface area between control volumes and volume of the control volume depicted in Figure 4. The discretization of the partial differential equation (18) is done with an implicit finite difference scheme. Crank-Nicolson formulation is used because it gives the smallest accumulated truncation error and an unconditionally stable linear system. In adimensional form, the energy balance for node j at position i and time step t+1 results in the following expression:

$$T_j^{i,t+1} - T_j^{i,t} = Fo_j^{i,t+1/2} \cdot \left[\left(T_j^{i+1,t} - 2T_j^{i,t} + T_j^{i-1,t} \right) + \left(T_j^{i+1,t+1} - 2T_j^{i,t+1} + T_j^{i-1,t+1} \right) \right] + \Omega_j^{i,t+1/2} \tag{19}$$

Here *Fo* represents Fourier's number defined by:

$$Fo_j^{i,t+1/2} = \left(\frac{\tilde{\kappa}_{\tau}}{\tilde{\rho} \cdot \tilde{C}p} \right)_j^{i,t+1/2} \cdot \frac{\Delta t}{(\Delta h_j)^2} \tag{20}$$

where Δt is the time step increment and Δh_j the distance between two adjacent nodes. For a better adimensional modeling, a constant grid spacing is

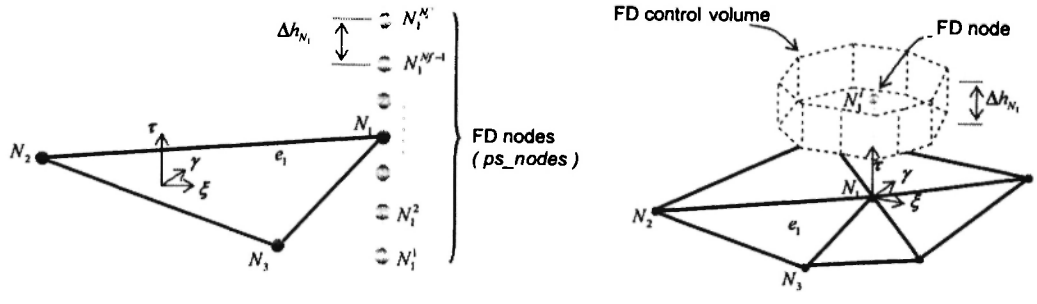

Fig. 3: Because conforming finite elements are used in the heat transfer formulation, the coupling between 2D in-plane and 1D gapwise solutions is done via the control volume of the FD nodes defined by the centroids and mid-edges of connected elements.

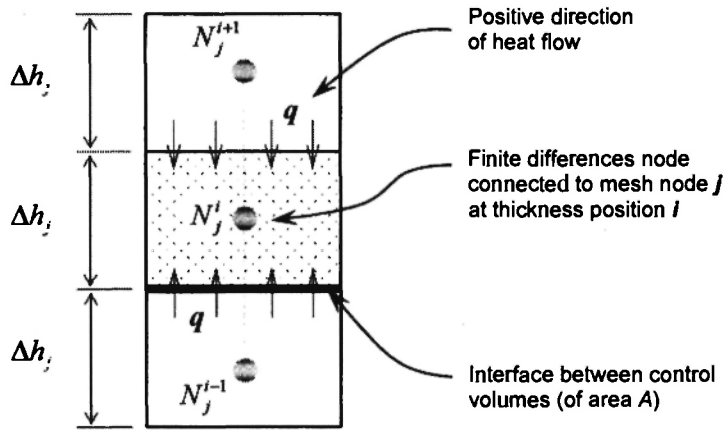

Fig. 4: Control volume of the one-dimensional finite difference approximation.

assumed for the through-thickness finite difference nodes. The term Ω_j^i in equation (19) is the heat generated by the resin exothermy in the control volume; it is expressed by:

$$\Omega_j^{i,t+1/2} = \left(\frac{\partial \alpha}{\partial t} \cdot \frac{\phi \ \rho_r}{\bar{\rho} \ \bar{C}p} \right)_j^{i,t+1/2} \Delta t \ H_{Tot} \quad (21)$$

The calculation of $Fo_j^{t+1/2}$ and $\Omega_j^{i,t+1/2}$ requires the knowledge of the spatial and temporal averaged properties in the control volume. If thermal properties do not strongly vary between two time steps, equation (19) reduces to:

$$T_j^{i,t+1}\left(1+2Fo_j^{i,t}\right) - T_j^{i+1,t+1}Fo_j^{i+1,t} - T_j^{i-1,t+1}Fo_j^{i-1,t} \quad (22)$$
$$= T_j^{i,t}\left(1-2Fo_j^{i,t}\right) + T_j^{i+1,t}Fo_j^{i+1,t} + T_j^{i-1,t}Fo_j^{i-1,t} + \Omega_j^{i,t}$$

For a group of finite difference nodes connected through the thickness, the solution is expanded into the following matrix notation:

$$\begin{bmatrix} 1 & 0 & 0 & 0 & \cdot & \cdot & 0 \\ -Fo^1 & 1+2Fo^2 & -Fo^3 & 0 & & & \cdot \\ 0 & \cdot & \cdot & \cdot & & & \cdot \\ \cdot & & \cdot & \cdot & \cdot & & \cdot \\ \cdot & & & \cdot & \cdot & \cdot & 0 \\ \cdot & & & 0 & -Fo^{Nf-2} & 1+2Fo^{Nf-1} & -Fo^{Nf} \\ 0 & \cdot & \cdot & 0 & 0 & 0 & 1 \end{bmatrix}_j^t \cdot \begin{Bmatrix} T^1 \\ T^2 \\ \cdot \\ \cdot \\ \cdot \\ T^{Nf-1} \\ T^{Nf} \end{Bmatrix}_j^{t+1} = \quad (23)$$

$$= \begin{Bmatrix} T^{wall\_top,t+1} \\ T^{2,t}\left(1-2Fo^{2,t}\right) + T^{3,t}Fo^{3,t} + T^{1,t}Fo^{1,t} + \Omega^{2,t} \\ \cdot \\ \cdot \\ \cdot \\ T^{Nf-1,t}\left(1-2Fo^{Nf-1,t}\right) + T^{Nf,t}Fo^{Nf,t} + T^{Nf-2,t}Fo^{Nf-2,t} + \Omega^{Nf-1,t} \\ T^{wall\_bot,t+1} \end{Bmatrix}_j$$

where j denotes the in-plane mesh node where finite differences are extrapolated, and Nf is the total number of finite difference nodes. To avoid confusion between FE and FD entities, the finite difference nodes are renamed *pseudo nodes* because they do not necessary represent the part geometry. In fact, the 1D Fourier's equation is adimensionally represented as a percent of the part thickness at the mesh node position. The vector $\{T^i\}_j^{t+1}$ represents the unknown temperatures of the *pseudo nodes* at time step t+1. The boundary conditions $T^{wall\_top,t+1}$ and $T^{wall\_bot,t+1}$ are imposed at time step t+1, i.e. imposed as the reference temperature of the top and bottom mold walls respectively.

Experimental studies of LCM processing have shown that significant temperature fluctuations appear at the mold walls during the filling and curing phases /2/. This implies that the assumption of a constant mold wall temperature is not always verified. To account for appropriate thermal boundary representation, different types of boundary conditions are considered. As shown in Figure 5, the mold wall can include a heating/cooling duct pipe at a distance d from the mold surface. The following general thermal boundary condition may then be applied:

$$k_{eff}\frac{\partial T}{\partial \tau} + h_{eff}\left[T^{wall} - T_{ref}(t)\right] = 0 \quad \text{for } \tau = 0, h_j \tag{24}$$

where T^{wall} is the temperature of the mold wall, and T_{ref} is a reference temperature of the fluid in the duct pipe. The coefficients k_{eff} and h_{eff} represent respectively the effective mold thermal conductivity and the convective heat transfer coefficient between the fluid and the pipe. The approximation of a constant mold wall temperature can be derived from equation (24) by setting:

$$T^{wall} = T_{ref}^t \tag{25}$$

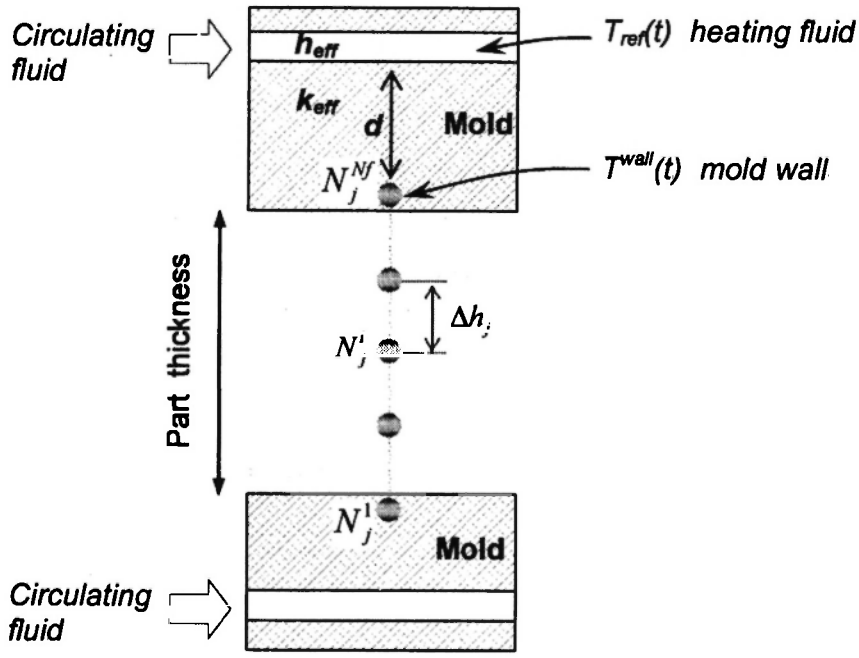

Fig. 5: One-dimensional finite difference grid through the part thickness. The mold walls are heated or cooled by duct pipes maintained at a known reference temperature T_{ref}.

where T^{wall} represents the temperature of the top or bottom mold surfaces, and T^{t}_{ref} is the mold platen reference temperature which varies in time. In this case, both temperatures are identical. A second boundary condition can be derived from the quasi-steady-state analysis of the mold heating/cooling system of Figure 5. This configuration results in the following equation:

$$\frac{T^{wall} - T^{i}_{j}}{d} + \left(\frac{h_{eff}}{k_{eff}}\right) \cdot \left[T^{wall} - T^{t}_{ref}\right] = 0$$

for $i = 2, Nf\text{-}1$ (26)

Regrouping terms, the expression of T^{wall} for a given time step $t+1$ will be:

$$T^{wall,t+1} = \left(T^{t+1}_{ref} \cdot (h_{eff} / k_{eff}) + T^{i}_{j} / d\right) \Big/ \left(d + h_{eff} / k_{eff}\right)$$

for $i = 2, Nf\text{-}1$ (27)

This approach represents fairly well the interactions between the mold walls and the surface of the part, although it is limited to the quasi-steady-state solution. This means that the temperature variations of the mold platens in time must be slow enough to allow a steady heat flow through the mold walls. In a more general case, it is necessary to solve a non-steady-state temperature evolution between the mold wall and the heating/cooling pipes. This problem can be solved by adding a finite difference grid into the mold walls and using an experimental value of the convection coefficient h_{eff}.

The accuracy of the solution of equation (23) depends on the choice of Fourier's number *Fo* (or Δt). Even if the Crank-Nicolson scheme is unconditionally stable, a choice of *Fo* close to unity tends to minimize the accumulated truncation error. In this work, an adaptative time step algorithm was implemented to provide a Fourier's number close to one. This algorithm calculates the time step Δt required to obtain a value of *Fo* close to unity. Because the thermal properties of the composite depend on both the temperature and the resin degree of cure, Fourier's number is expected to vary through the thickness of the part. From all the values of *Fo* calculated for a stack of finite difference volumes, the adaptative time step algorithm selects the one that results in the minimum value of Δt required for convergence.

During composite processing, the exothermic chemical reaction of resin polymerization causes a quick temperature increase in the core of the part. The temperature rate $\partial T/\partial t$ between two time steps may become high enough to generate numerical oscillations and alter the calculated temperature profile through the thickness. Therefore, it is necessary to decrease the time step in order to keep the desired accuracy of the numerical solution. In the particular case of LCM, this can be achieved by setting Δt as a function of temperature and the cure rate $\partial\alpha/\partial t$ with the following empirical condition:

$$\frac{\partial \alpha}{\partial t} T \approx \frac{\Delta \alpha}{\Delta t} T \leq 1 \qquad (28)$$

NUMERICAL IMPLEMENTATION OF THE HYBRID FE/FD MODEL

In /17/, a methodology was presented to solve the inconvenience of multi-material definition of the laminated preform. Isothermal three-dimensional flows were calculated by constructing automatically with an extrapolation algorithm, non-conforming finite elements from the two-dimensional mesh. Beginning with a thin shell mesh, a solid mesh is generated by extruding the 2D finite element mesh. The extrusion is defined by the preform stacking sequence that allows the use of different material properties for each laminate ply. This methodology can also be applied to generate parallel layers of two-dimensional elements not coupled with the through-thickness direction. As depicted in Figure 6, different levels of inter-layer coupling are possible when the mesh extrapolation is combined with the one-dimensional finite difference grid. As already mentioned, the simulation of LCM processes involves in complex coupling between pressure, temperature and degree of cure. Two or three-dimensional solutions are required depending on to the level of coupling between the different physical phenomena that came into play in LCM process. It is common practice in computer simulation to begin with simple models so as to understand the global flow evolution and verify the

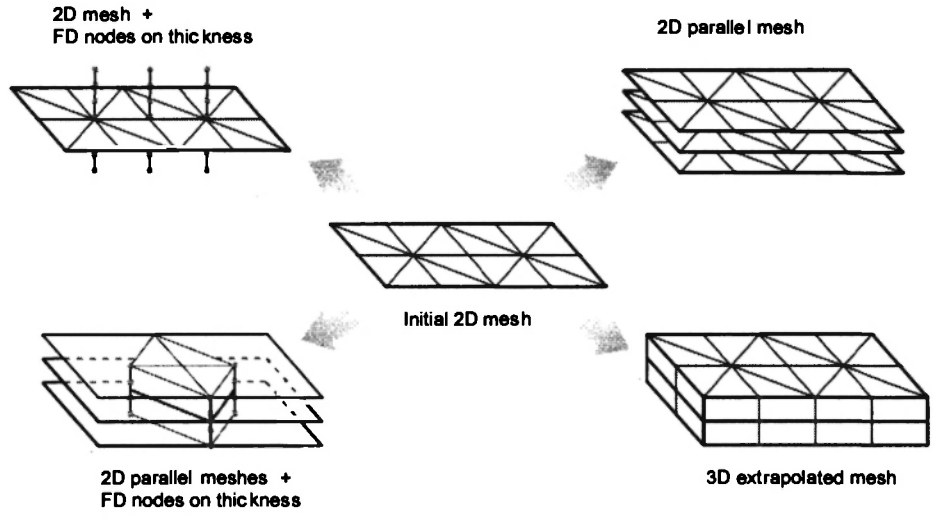

Fig. 6: Different levels of inter-layer coupling with the mesh extrapolation algorithm and the 1D finite difference grid.

geometrical model. Then, model refinement is carried out and more elaborated mathematical formulations are progressively implemented. Finally, complex mathematical and geometrical models are resolved to predict accurately the filling and curing stages. In this iterative process, the remeshing of 3D geometries is a complex task especially when thermal boundary conditions have to be specified on a three-dimensional mesh.

In this investigation, an integrated methodology is proposed to analyze the level of complexity of the numerical and geometrical models. As shown in the schematic representation of Figure 7, various levels of coupling may be obtained by combining the finite element mesh with the finite difference grid. The numerical formulations presented in this paper stand for the following solutions:

- Flow analysis (Darcy and filling):
  - 2D and 3D finite elements
- Heat conduction (energy balance):
  - 2D and 3D finite elements
  - 2D finite elements + 1D finite differences
- Transport equation (balance of chemical species):
  - 2D and 3D finite elements
- Resin cure:
  - 2D and 3D finite elements
  - 2D finite elements + 1D finite differences

The possible combinations between these approximations are listed in Table 1. Different levels of integration of the flow, thermal and curing formulations are possible. In the simplest coupling, the flow is evaluated on the 2D mesh and the energy balance is studied with the 2D finite element space and 1D finite difference approximation. In a higher level of coupling, flow and transport are calculated on 2D parallel meshes, but pressure is not considered uniform in the through-thickness direction. Heat conduction and resin cure is solved on the parallel FE meshes and coupled across the thickness via the FD grid. The most complex formulation is the pure three-dimensional FE solution based on *prism6* extrapolated elements or tetrahedrons.

An algorithm was developed to perform compatible calculations on a series of parallel meshes. The pressure, temperature, degree of cure and viscosity are averaged and transferred between the FE and FD control volumes. The aim of this integrated methodology is to help in process design. Beginning with the same 2D mesh, global flows can be rapidly computed. More complex solutions may be performed without much user effort. It is well known that in numerical process optimization, the successive evaluations of complex geometrical models results in extremely high cpu times. The multiple coupling method has the ability to initially evaluate the global problem in a simple solution and

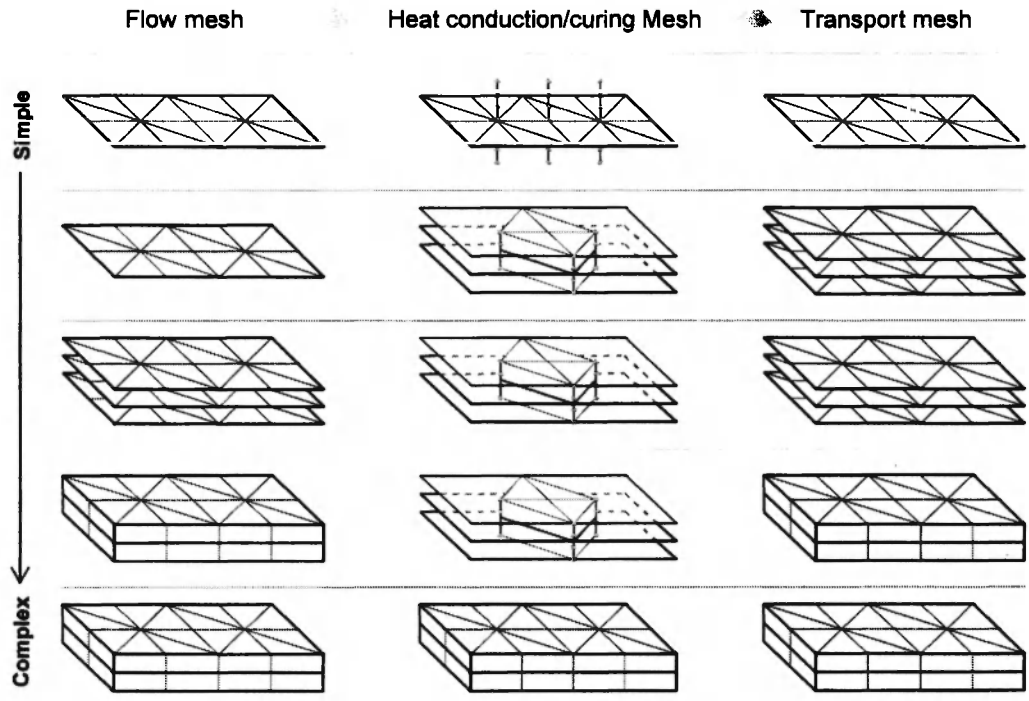

Fig. 7: Schematic representation showing increasingly complex integration of flow, conduction and transport solutions. Different levels degrees of coupling are obtained by combining FE meshes and FD grids.

Table 1

Different levels of integration of flow/thermal/curing formulations depending on the level of mesh coupling.

Model	Simple → Complex					
Darcy Pressure	NE FE	C FE	NE FE	C FE	C FE	C FE
Fluid Transport	NE FE	NE FE	NE FE	C FE	C FE	C FE
Heat Conduction	NE FE + FDT	NE FE + FDT	C FE	NE FE + FDT	NC FE + FDT	C FE
Viscosity	Averaged Thickness	Averaged Thickness	Averaged Thickness	Averaged Element	Averaged Element	Averaged Element
Kinetic reaction	FDT	FDT	C FE	FDT	FDT	C FE

NE FE : No mesh Extrapolation – Finite Element solution
NC FE : Non Coupled extrapolated mesh – Finite Element solution
C FE : Coupled extrapolated mesh – Finite Element solution
FDT : Through-Thickness Finite Differences solution

progressively increase the model complexity according to the optimization convergence. The method is promising and may turn full process optimization feasible. Figure 8 shows the flow chart used to solve the coupled equations of the non-isothermal filling/curing simulation.

ANALYTICAL VALIDATIONS

Case I: 3D heat conduction - steady-state

To validate the numerical solution of the heat equation, an analytical comparison is carried out in the tnree dimensional space. In this test case, a cubic geometry was selected to evaluate the steady-state heat conduction. As shown in Figure 9, the upper surface of the cube is maintained at a constant non null temperature while the bottom surface and two sides are assumed to have a zero constant temperature. Considering that thermal properties are all unity, the analytical solution of the stationary temperature profile is:

$$T(x,y,z)=\frac{16}{\pi^2}\sum_{n=0}^{\infty}\sum_{m=0}^{\infty}\frac{\sin\frac{(2n+1)\pi x}{L}\sin\frac{(2m+1)\pi y}{W}\sinh\pi z\sqrt{\frac{(2n+1)^2}{L^2}+\frac{(2m+1)^2}{W^2}}}{(2n+1)(2m+1)\sinh\pi H\sqrt{\frac{(2n+1)^2}{L^2}+\frac{(2m+1)^2}{W^2}}} \tag{29}$$

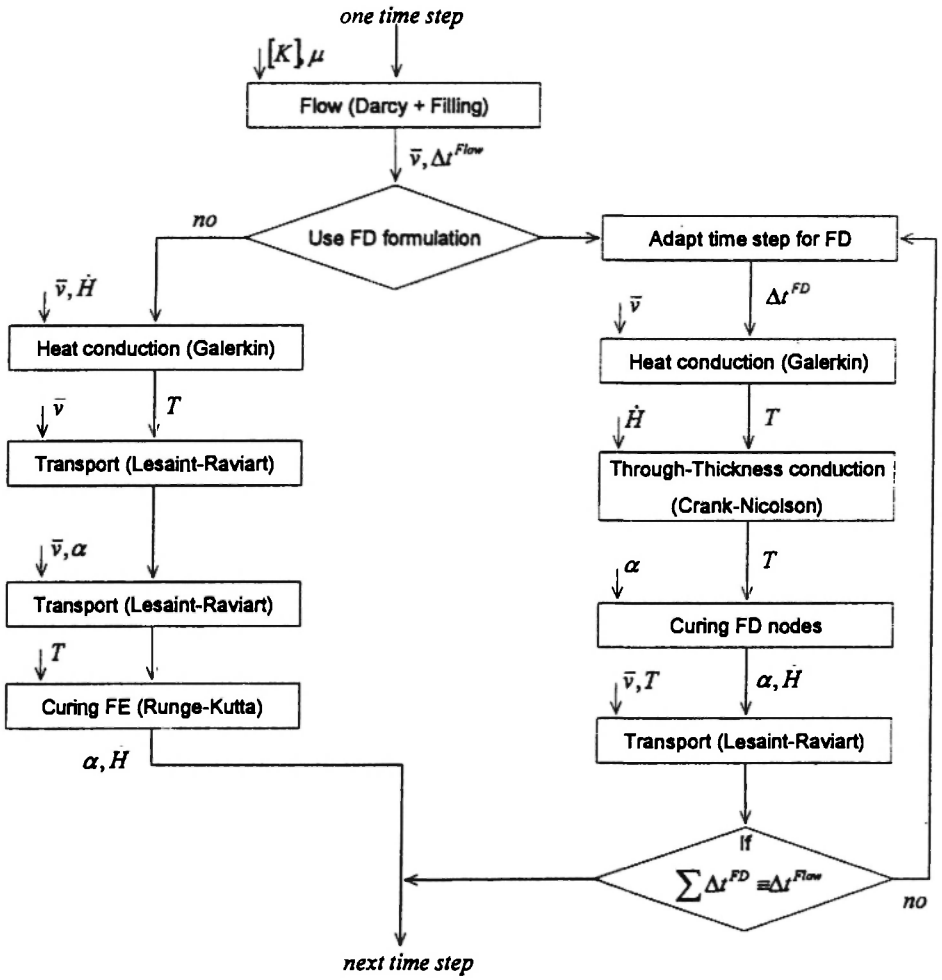

Fig. 8: Flow chart of the numerical algorithm for the non-isothermal analysis.

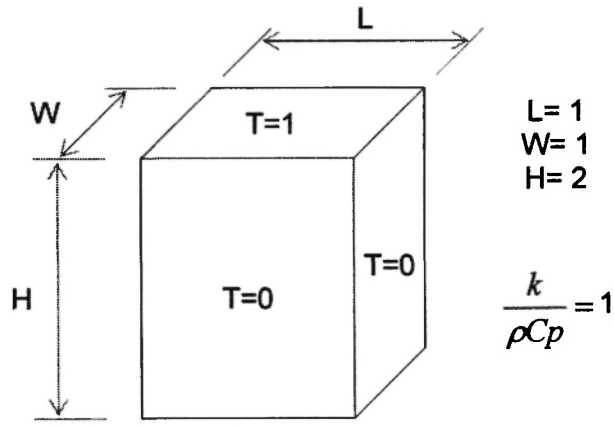

Fig. 9: Domain used for the validation test I.

where L, W and H are the cube dimensions. Two formulations were tested in the steady state: full 3D finite elements and hybrid 2D FE/1D FD. The geometrical support used for each formulation is depicted in Figure 10. To ensure a good aspect ratio of the *prism6* finite elements, the number of nodes in the transverse direction H is double that of the in-plane nodes. Note that non-connected layers of the hybrid FE/FD model are extrapolated at the midplane of the connected layers. Figure 11 shows the temperature distribution along the z-axis for $x= y= 1$. The theoretical temperature profiles are compared with the numerical simulations for both formulations. The 3D mesh consists of 5x5 nodes in the xy plane and 10 extrapolated layers. The hybrid mesh has only 5 FE layers, while the number of FD nodes in the z-direction was varied between 7 and 21. A good approximation of the analytical values was found for the pure FE solution. The hybrid formulation increases in accuracy with the number of finite difference nodes. A maximum relative error has been defined as the maximum error at a node point between the analytical and numerical solutions. The maximum relative error for different mesh sizes is shown in Figure 12. Due to the 3D behavior of heat conduction, the three spatial dimensions must be increased proportionally to compare the error between meshes. For the pure FE solution, the error decreases logarithmically when the number of mesh nodes is duplicated. The results of the hybrid FE/FD formulation are in good agreement with analytical values even for a coarse mesh. For the same mesh, an important gain in accuracy is observed when the FD nodes are duplicated.

Case II: 3D heat diffusion - un-steady-state

A two-dimensional heat diffusion analysis has been used to test the proposed thermal formulations. As

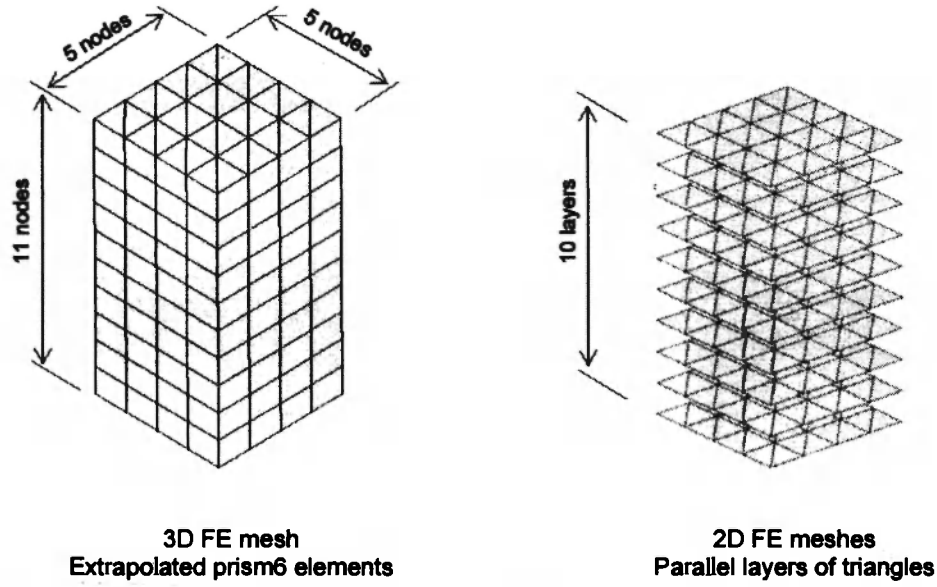

Fig. 10: Two meshes used for test case I: extrapolated parallel layers coincide with the midplanes of each connected layer.

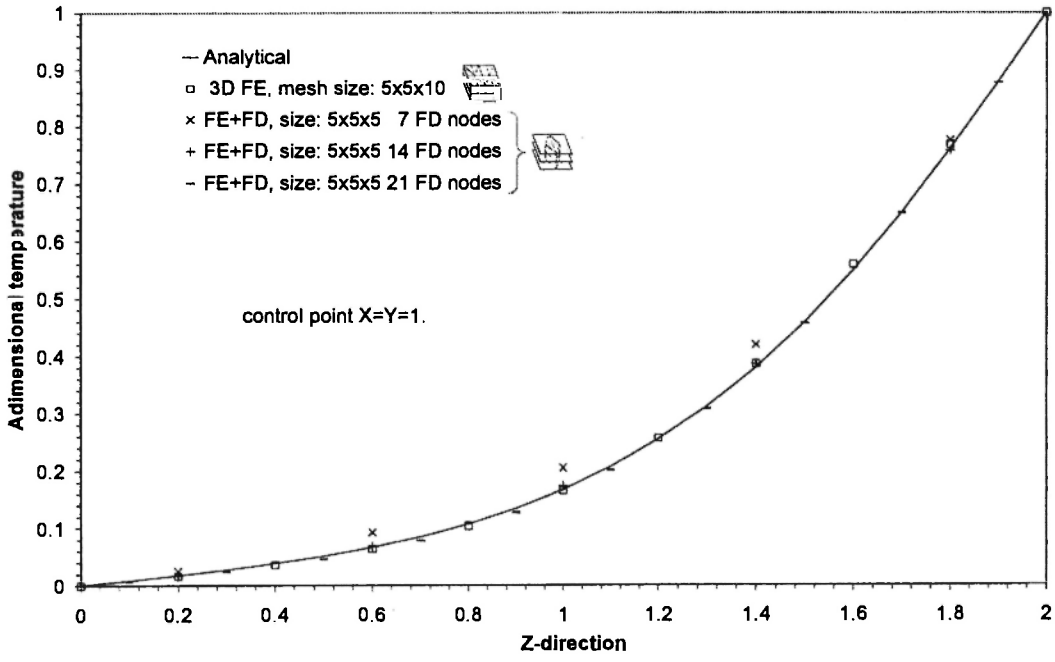

Fig. 11: Comparison of pure FE and hybrid FE/FD solutions with theoretical values for test case I.

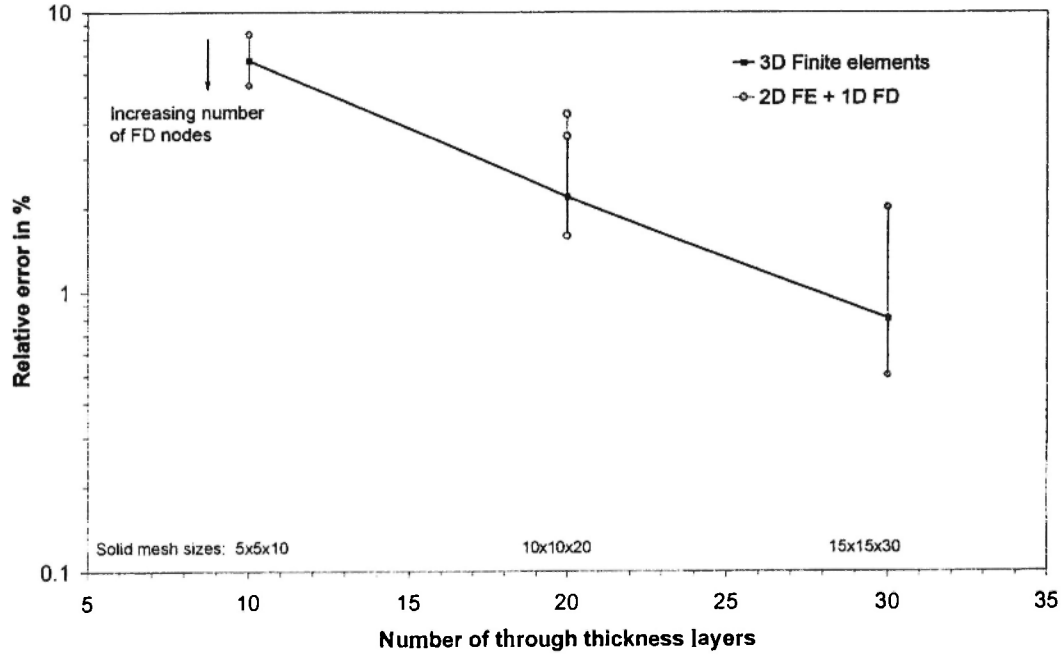

Fig. 12: Maximum error of both formulations obtained for different mesh and grid sizes in test case I.

depicted in Figure 13, a rectangular domain is considered to be at initial temperature T_0=0. A constant temperature is imposed at two sides of the rectangle $T(t)$=1. Also, the meshes generated to test the FE and hybrid FE/FD formulations are depicted in the same figure. The analytical solution can be found by the method of separation-of-variables /19/. The dimensionless temperature distribution may be expressed as the product of the solutions in each direction:

$$\left(\frac{T-T_\infty}{T_0-T_\infty}\right)_{X,Y}=\left(\frac{T-T_\infty}{T_0-T_\infty}\right)_X\cdot\left(\frac{T-T_\infty}{T_0-T_\infty}\right)_Y \qquad (30)$$

where T_0 is the initial temperature, and T_∞ the boundary condition outside the domain. A square is considered in this test with L= H= 1 and a constant boundary condition on two sides. The one-dimensional solution is applicable here to the X and Y axes, and may be written with a Fourier sine expansion as follows:

$$\left(\frac{T-T_\infty}{T_0-T_\infty}\right)_{X\text{ or }Y}=\frac{4}{\pi}\sum_{i=0}^{\infty}\frac{\sin(\psi_i\cdot x)}{\psi_i}\cdot\exp\left(-\psi_i^2\cdot\alpha\cdot t\right) \qquad (31)$$

$$\psi_i=\frac{2n+1}{L}\pi$$

where α is the thermal diffusivity of the material (in this case α=1). Finally, the theoretical solution is finally the combination of equations (30) and (31). The numerical simulation was performed using different mesh sizes and number of extrapolated layers. The number of elements in the gapwise direction was kept at one, while the ratio of the in-plane number of elements along the X and Y directions of the 3D mesh was maintained constant. Figure 14 depicts the temperature evolution at a control point X= Y= 1. Theoretical values are compared to the results of the pure FE and hybrid FE/FD solutions for two mesh sizes. The pure FE formulation shows a good agreement with analytical values even for a coarse mesh (5x5 nodes). The hybrid formulation for 5 extrapolated layers gives also a good approximation. When only one extrapolated layer is used, the solution seems to diverge from exact values.

The L_n-norm of the error between the temperature calculated at a given position ε and the theoretical solution is defined as:

$$L_n(\varepsilon)=\left(\sum_{t=1}^{I}\left|T_\varepsilon^{cal}(t)-T_\varepsilon^{exact}(t)\right|^n/I\right)^{1/n} \qquad (32)$$

where $T_\varepsilon^{exact}(t)$ and $T_\varepsilon^{cal}(t)$ are the exact and calculated temperatures at position ε and time t, and I denote the number of time steps. A mesh refinement study has been performed to evaluate the influence of the mesh on the rate of convergence. Figure 15 shows the L_2-norm of the error for each mesh size. An error of less than 2% was found for the pure FE formulation when using a mesh of 5x5 nodes. The error decreased to around 1% for a 30x30 mesh. In the hybrid formulation, the error with one mesh layer of 5 nodes and finite differences in the transverse direction was 4.5%. Increasing the number of extrapolated layers, the number of transverse FD nodes was duplicated resulting in higher convergence rates. The accuracy of the hybrid solution for a mesh of 10 nodes along the X-axis, 10 extrapolated layers and 20 FD nodes was 0.15%. These

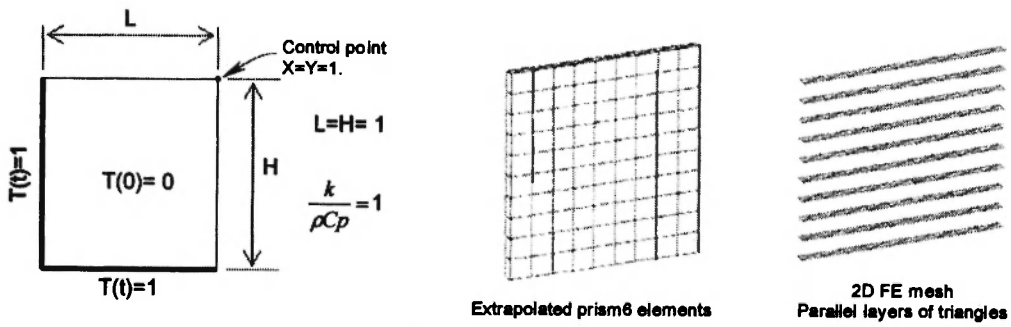

Fig. 13: Rectangular domain used for validation test II and display of the 3D and parallel layers meshes.

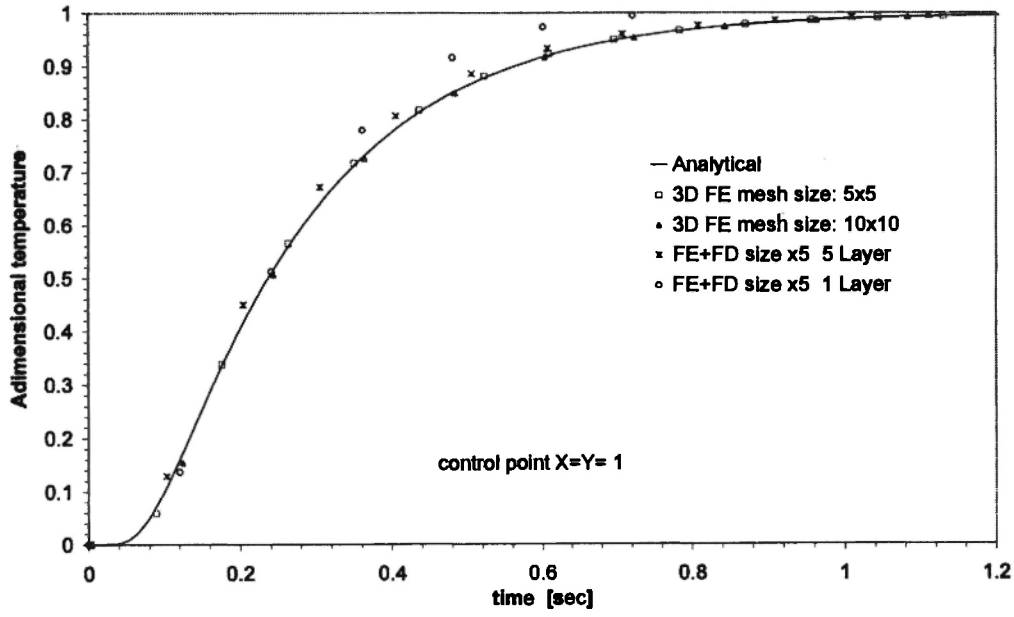

Fig. 14: Comparison with analytical values of adimensional temperature at point $X=Y=1$ for pure FE and hybrid FE/FD solutions (test case II.).

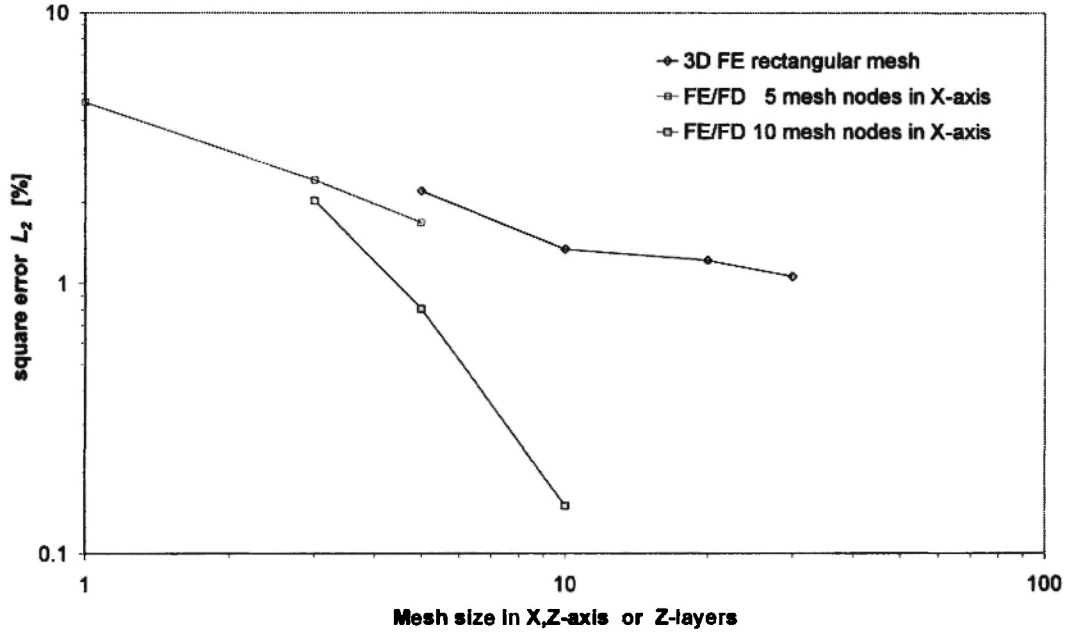

Fig. 15: Convergence for 3D mesh refinement and parallel layers increment. The rate of convergence increases more with the number of layers (FE/FD solution) than with the number of nodes (FE solution). Note that the number of finite difference nodes is twice the number of layers.

results show that both formulations converge to the theoretical values even for coarse meshes. The hybrid formulation gave increased convergence rates than the three-dimensional FE solution.

Case III: heat diffusion with source term - curing analysis

One of the most important analyses in LCM concerns the prediction of the chemical conversion during the exothermic polymerization. To test the quality of the numerical formulations, a curing test was carried out in a rectangular cavity similar to test case II. The cavity has dimensions 0.1 m length, 0.05 m thickness and 0.005 m width. A mix of 50 % resin and fibers is considered to be initially at 300°K. In the top and bottom surfaces, a mold temperature of 400°K was fixed. On one side of the cavity, a temperature of 350°K was set to induce an in-plane heat flow. The kinetic modeling of the resin and the thermal properties of the fibers and resin are presented in Table 2. In a typical LCM curing of thick composite parts, in-plane heat flow plays an important role in the evolution of resin polymerization. This heat flow induces a non-uniform conversion rate in the part that results in residual stresses and geometrical distortions. In the cavity tested, a control point located at the centre is used to compare the differences in the exothermic temperature and degree of cure between numerical formulations. Figure 16 shows the pure FE and hybrid FE/FD solutions of temperature and degree of cure at the control point. In absence of an analytical solution, a refined two-dimensional finite elements solution is used as reference. For the same number of mesh and FD nodes, the hybrid formulation seems to better approximate the two-dimensional solution. This is mainly because the control volumes are defined coincident with the elements and the curing formulation uses an averaged element temperature to evaluate the resin kinetics. The FD formulation considers the control volumes associated to each node, and uses the nodal temperatures for kinetic calculations. To compare these results, an error estimator of the computed curing time (R_c) may be defined as follows:

$$R_c = \frac{\left| t_c^{ref} - t_c \right|}{\Delta t^{ref}} \tag{33}$$

Table 2

Kinetic model and thermal properties used in test case III.

Kinetic Model	$\frac{d\alpha}{dt} = \left(A_1 \cdot \exp\left(\frac{-E_1}{T} \right) \alpha^m \right) \cdot (1-\alpha)^p$		
Property	**Units**	**Resin**	**Fibers**
Density	Kg/m3	1000	2500
Specific Heat	J/Kg °K	1500	800
Heat conductivity	W/m °K	0.25	0.25
Heat of reaction	KJ	250	-
A_1	1/sec	1.0	-
E_1	°K	1400	-
m	-	1.2	-
p	-	0.8	-

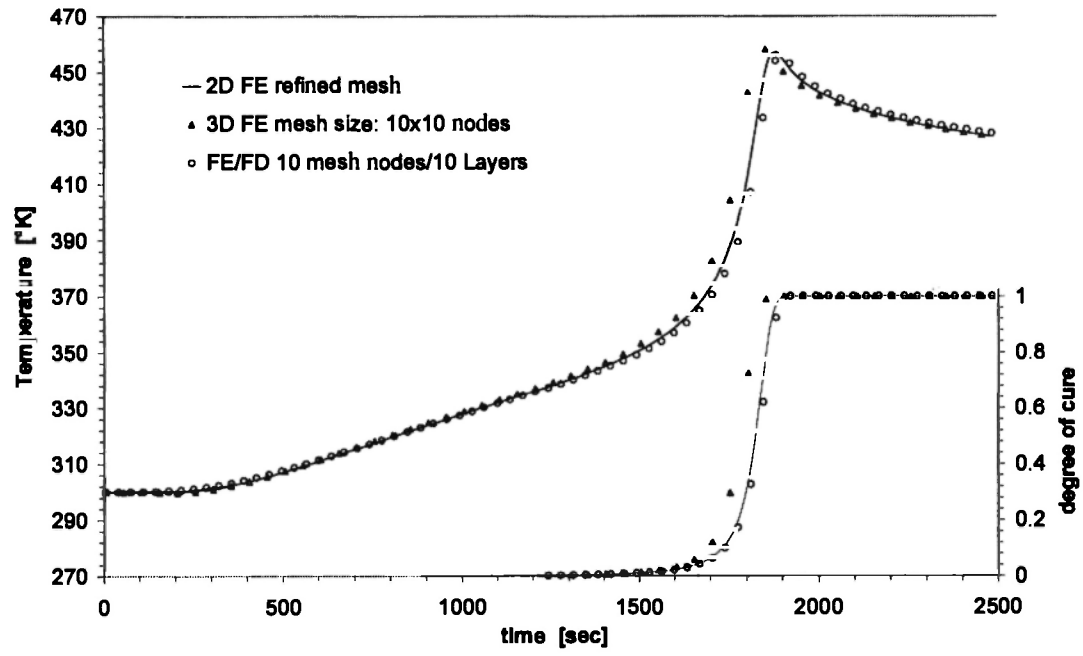

Fig. 16: Evolution of temperature and cure profiles at the cavity centre is depicted for pure finite elements and hybrid FE/FD solutions. The 2D FE solution is used as reference.

where t_c is the calculated time to fully cure the cavity, t_c^{ref} is a reference time considered to be the curing time calculated by the two-dimensional solution. Δt^{ref} is a reference time variation ($\Delta t^{ref} = 60$ sec.). The resulting error on the curing time for different mesh sizes is given in Figure 17. For the same number of layers and FD nodes, the hybrid FE/FD formulation shows a smaller error than the pure FE formulation. The error decreases logarithmically for both formulations when the number of through-thickness layers increases. To estimate the performance of the solutions, the computer time is combined with the error on curing time in the following form:

$$R_P = (1 - R_c) \cdot (1 - R_{cpu}) \tag{34}$$

where

$$R_{cpu} = t_{cpu} / t_{cpu}^{ref} \tag{35}$$

Here t_{cpu}^{ref} and t_{cpu} denote respectively a reference cpu time and the cpu time to calculate a given solution. Figure 18 shows the performance index R_P for different solutions of both models. For coarse meshes, the gain in cpu time is compensated by the important error of the solution, resulting in a worse performance. When the number of through-thickness layers or finite difference nodes is increased, the performance shows a peak for around 15 layers. In all cases the hybrid formulation gives an improved performance with respect to the pure FE solution. This is due to the quality of the FD calculations and the fast solution of the tri-diagonal linear systems of the hybrid formulation. After the peak, the mesh or grid refinement results in a decrease of performance. The decay of the FE solution is more pronounced than for the hybrid formulation due to time consuming inversion of sparse FE matrices. In conclusion, the hybrid formulation presents strong advantages in terms of performance compared to pure FE techniques.

Case IV: heat convection test

In order to analyze the effects of the heat convection during filling, a linear injection in a heated cavity is considered. As depicted in Figure 19, the 0.5 *m* length rectangular cavity has a constant thickness of 5 *mm*.

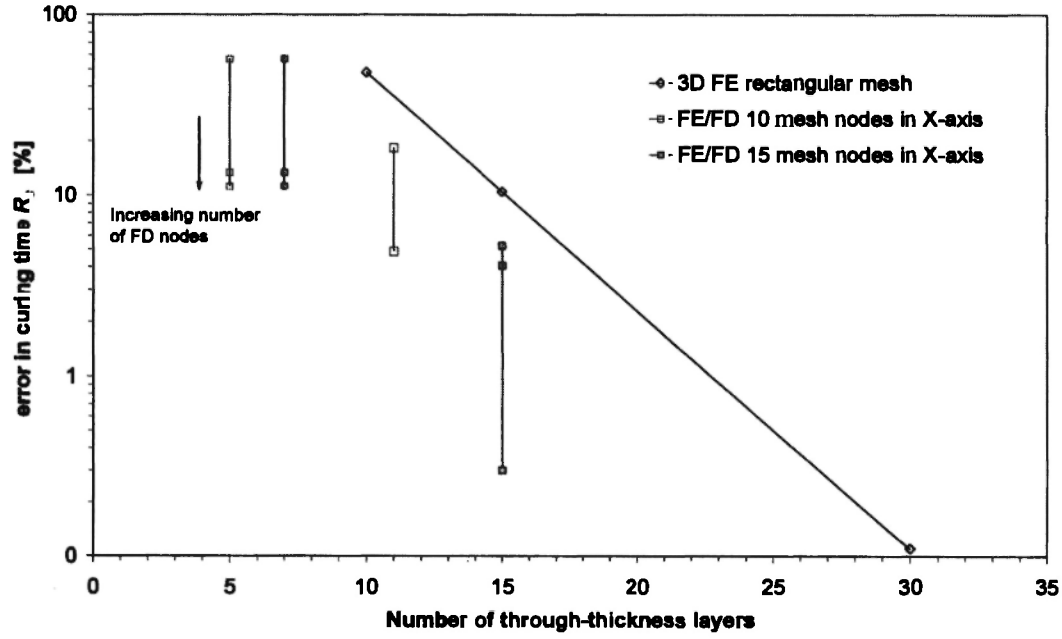

Fig. 17: Comparison of error in the estimation of curing time for different mesh sizes. The hybrid formulation gives a better approximation than pure finite elements for the same number of trough-thickness layers.

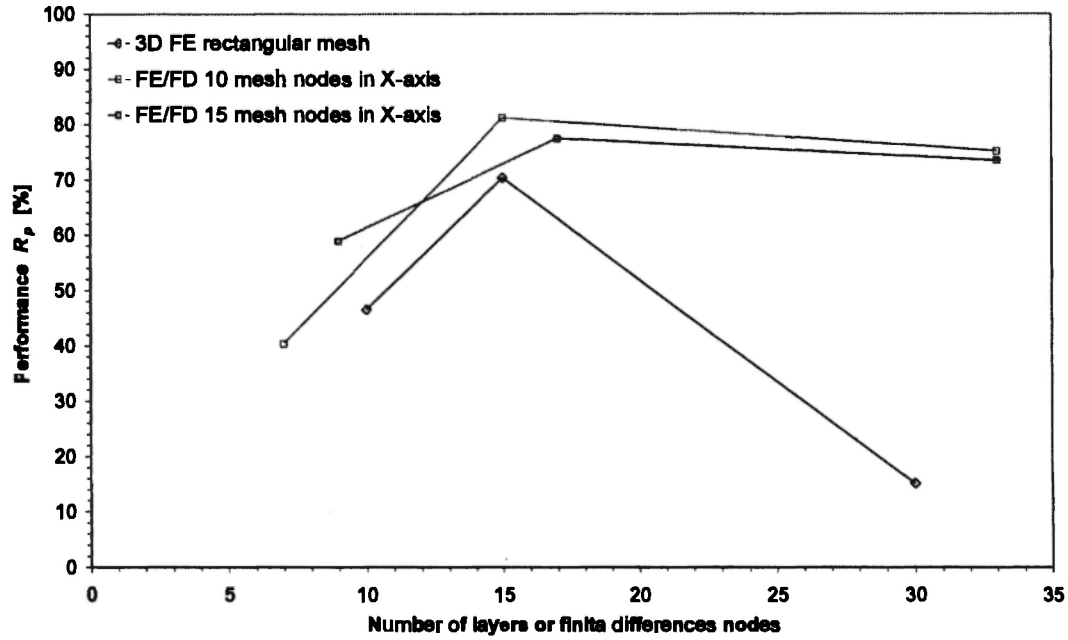

Fig. 18: The performance of diver solutions is compared for various meshes with increased number of through-thickness layers of finite differences nodes. The hybrid formulations seem to give a better performance for curing analyses.

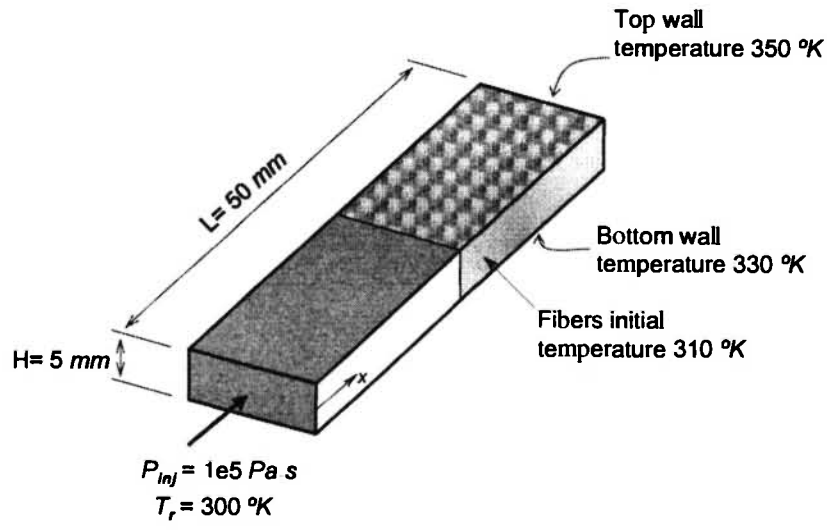

Fig. 19: Rectangular cavity used for the 2D convection test with different top and bottom mold wall temperatures.

Temperature is fixed at the top and bottom surfaces of the mold at 350 °*K* and 330 °*K* respectively. A fiber reinforcement with an isotropic permeability of 1e-10 m^2 is considered to fill the cavity with a fiber bed of volume content 50%. The thermal properties of the fibers and resin are the same as in the previous cases (see Table 2). The initial temperature of the fibers is 310 °*K* while the resin is injected into the cavity at 300 °*K* with a constant pressure of 1e5 *Pa*. To evaluate the pure heat transport, the resin viscosity is considered to be constant with temperature at a value of 1 *Pa.s*. As a result of the linear flow in the rectangular cavity and the transverse heat conduction, a non-uniform heat convection will appear across the cavity thickness. In order to solve this heat transport problem, different models were generated combining FE and FD formulations supported by 2D and 3D finite elements. As shown in Table 3, six models are presented to account for various FE/FD combinations. Models #1 and #2 are the standard solutions used in the previous LCM simulation code for 2D and 3D analyses respectively. Model #3 is the new proposed 3D pure FE solution based on *prism6* elements, while models #4 to #6 are the new simplified solutions combining FE with FD formulations.

Table 3
Combination of different formulations and elements used for test case IV.

Model	#1	#2	#3	#4	#5	#6
Formulation	FE	FE	FE	FE+FD	FE+FD	FE+FD
Finite Element	triangles	tetrahedrons	prism6	triangles	triangles	triangles+prism6
Heat solution	2D	3D	3D	2D+1D	2D+1D	2D+1D
Transport	2D	3D	3D	2D	2D	3D
Nbr. of layers	20	10	10	1	5	10
Nbr. of FD nodes	-	-	-	10	10	12
Status in the code	in use	in use	new	new	new	new

Figure 20 shows the temperature evolution on a fixed position along the longitudinal axis (x= 30 *mm*) for the six models tested. At the beginning, the temperature evolves due to through-thickness conduction. At around 20 seconds, the flow front arrives to the fixed position inducing a temperature increment due to the heat transport. While during the conduction period the models are reasonably close to each other, in the heat convection regime a maximum variation of 2 °*K* appears between the 2D solution of model #1 and the FE/FD models #5 and #6. The simplest solution of one layer of 2D finite elements and through-thickness finite differences (model #4) shows a small overheating at the flow front arrival, and then converges to the stabilized value of models #5 and #6. Figure 21 depicts the temperature distribution in the cavity midplane at the end of filling for the six models tested. Nearly the injection side, where the heat flow is convection dominated, variations were found between models. Combined FE/FD formulations on a coarse mesh show a delay in the temperature evolution with respect to the 2D solution of model #1 obtained on a refined mesh. The 3D pure finite element solutions of models #2 and #3 are more accurate than the 2D heat transport of models #4 to #6. For the same number of layers, the new *prism6* element gives a better solution than the tetrahedrons model. Note that in the stabilized regime, a temperature oscillation appears in the tetrahedron solution because the velocity vector is outside the plane of the elements. This effect disappears in the *prism6* solution because the velocity is aligned with the element plane.

Table 4 gives the computer times required to run each model on an IBM IntelliStation Z-Pro PC with a Pentium IV (2.8 GHz) processor. While the standard tetrahedrons solution took more than 4300 seconds to run, the new *prism6* model required only 1700 seconds for an improved solution. The 2D FE/1D FD models #4 and #5 show an important advantage in terms of cpu times (simulations in 24 and 280 seconds respectively). This analysis shows that even if the quality of the 2D FE/1D FD is not as precise as the pure 3D finite element solution, the gains in computer time make the simplified model reliable for a first approximation of the flow solution. Depending on the complexity of the flow, the model quality can be progressively increased to approach the solution. The simplified model can initially be used to evaluate the global problem in order to optimize the filling and/or curing stages. As the numerical optimization algorithm progresses, model complexity can be increased to improve the accuracy of the local optimum.

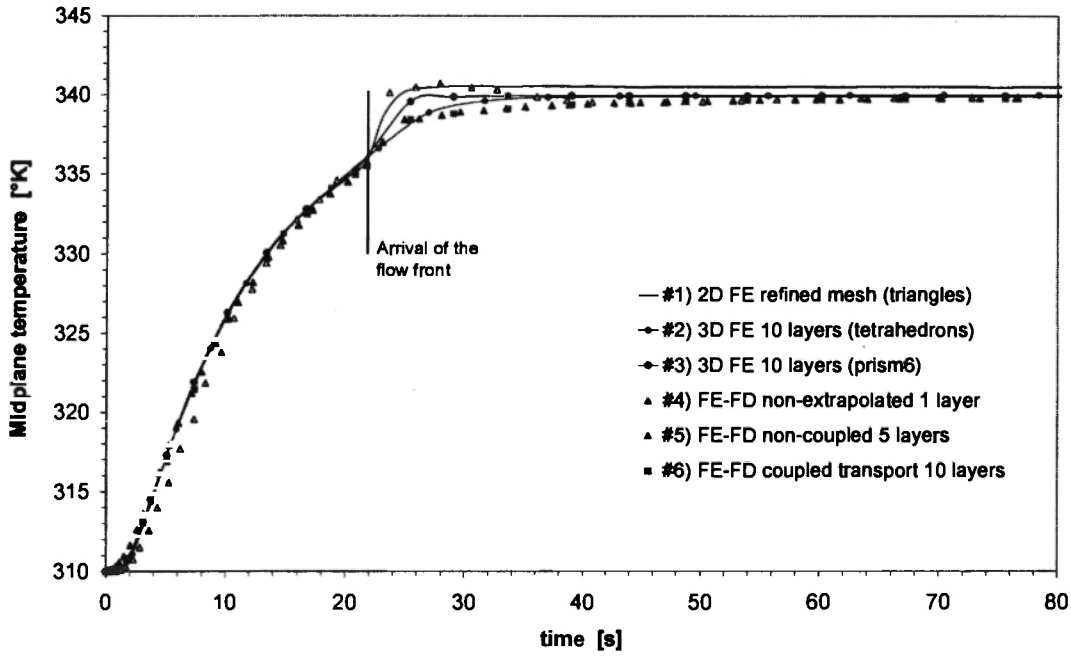

Fig. 20: Temperature evolution at the control point for the six solutions tested.

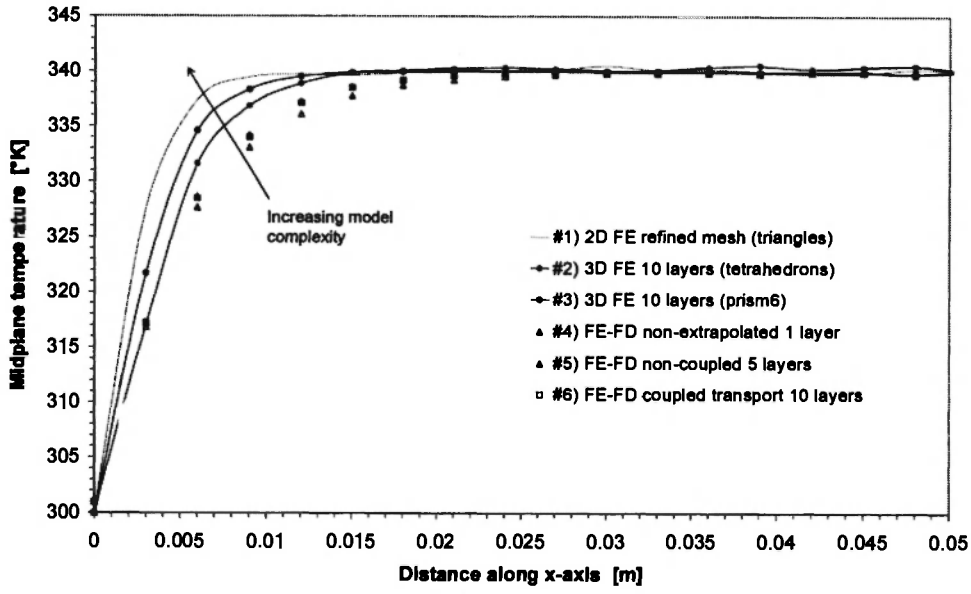

Fig. 21: Temperature distribution at the end of filling along the cavity midplane for the six solutions tested.

Table 4

Computer times required to calculate for each solution of test case IV (times are in seconds).

Model	#1	#2	#3	#4	#5	#6
Finite Element	triangles	tetrahedrons	prism6	triangles	triangles	triangles+prism6
Flow cpu time	167.6	1135.1	1474.4	14.9	51	1184
Heat cpu time	668.1	3211.4	223.5	5.8	211.2	221.2
In/output time	2.9	1.1	3.4	1.2	9.2	6.8
Tolat cpu time	**853.8**	**4378.2**	**1712**	**24.1**	**283.6**	**1439.3**

CASE STUDY – AUTOMOTIVE FRONT HOOD

To illustrate the advantages of the proposed models and of the extrusion methodology, non-isothermal filling and curing simulations of an automotive front hood have been conducted. As depicted in Figure 22, the mid-plane geometry of the front hood is discretized with a 2D finite element mesh containing 3000 triangular elements and 1600 nodes. The dimensions of the part are approximately 1.56 *m* length by 1.15 *m* width with 5 *mm* thickness. During the non-isothermal filling, the resin is injected at a constant pressure of 3e5 *Pa* at 330 °*K*. The mold cavity contains an isotropic fiber mat with a permeability of 1e-9 m^2 (V_f= 50%). The fibers are considered to be preheated at 350 °*K* while a fixed temperature 370 °*K* is set on the top and bottom mold walls. To account for the resin polymerization during the filling flow, the resin viscosity was modeled as dependent of the temperature and the degree of conversion (see Table 5). The thermo-kinetic parameters used in the simulation are listed in Table 2. As presented in Table 6, five models were selected to run the non-isothermal filling followed by a curing phase. Pure FE solutions are calculated with a tetrahedron

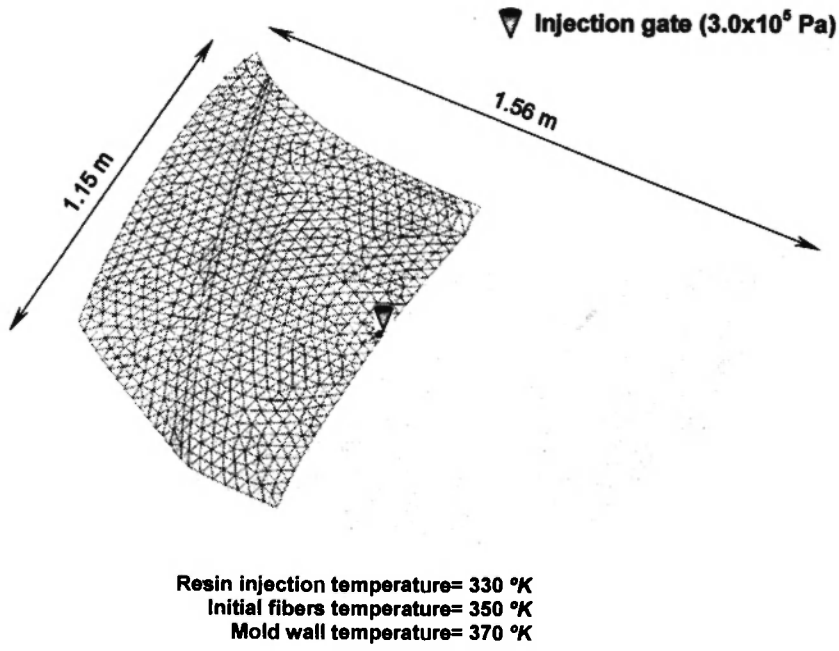

Fig. 22: Midplane geometry and finite element discretization of the automotive hood used for the case study.

Table 5

Rheological model used in the non-isothermal simulation of the automotive front hood.

Rheological Model	$\mu(T,\alpha) = A_\mu \cdot \exp\left(\frac{E_\mu}{T} + B_\mu\,\alpha\right)$	
Coefficient	**Units**	**Value**
A_μ	Pa.s	0.0001
E_μ	°K	2500
B_μ	-	2.8

Table 6

Description of the five models used to compute the non-isothermal filling and curing of the automotive front hood.

Model	**#1**	**#2**	**#3**	**#4**	**#5**
Formulation	FE	FE	FE+FD	FE+FD	FE+FD
Finite Element	tetrahedrons	prism6	triangles	triangles	triangles+prism6
Heat solution	3D	3D	2D+1D	2D+1D	2D+1D
Transport	3D	3D	2D	2D	3D
Nbr. of layers	5	5	1	1	3
Nbr. of FD nodes	-	-	3	5	7

mesh (model #1) and a *prism6* mesh (model #2). Three combined FE/FD formulations are proposed. The first two (models #3 and #4) are the simplest solution consisting of one layer of 2D finite elements (triangles) to evaluate the in-plane fluid flow and heat transport, coupled with 1D through-thickness finite differences to account for the transverse conduction. Model #5 combines the 2D FE and 1D FD heat conduction (triangles) with 3D heat and flow transport in *prism6* elements.

Figure 23 shows the flow front locations in time for the non-isothermal filling simulation of models #1, #2, #4 and #5. A good agreement was found between the models. A maximum predicted filling time of 590 seconds was obtained for the hybrid 3D FE/FD formulation of model #5 versus 540 seconds of the pure 3D FE solution with *prism6* elements (model #2). Figure 24 depicts the degree of resin conversion calculated at the midplane of the cavity at the end of filling. As expected, the resin at the flow front has the

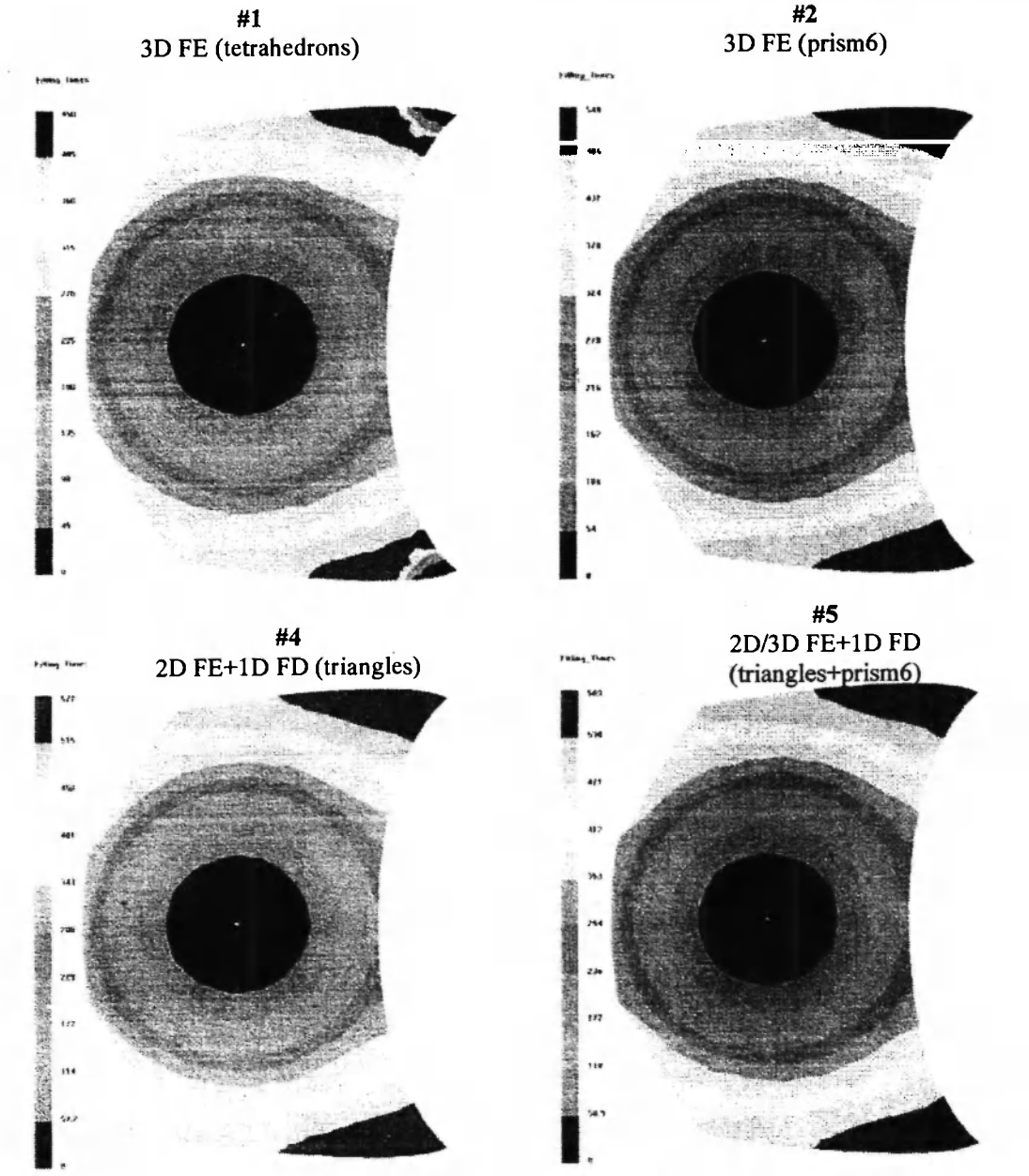

Fig. 23: Flow front position in time for the non-isothermal mold filling of an automotive front hood. The solutions of four solution tested are depicted.

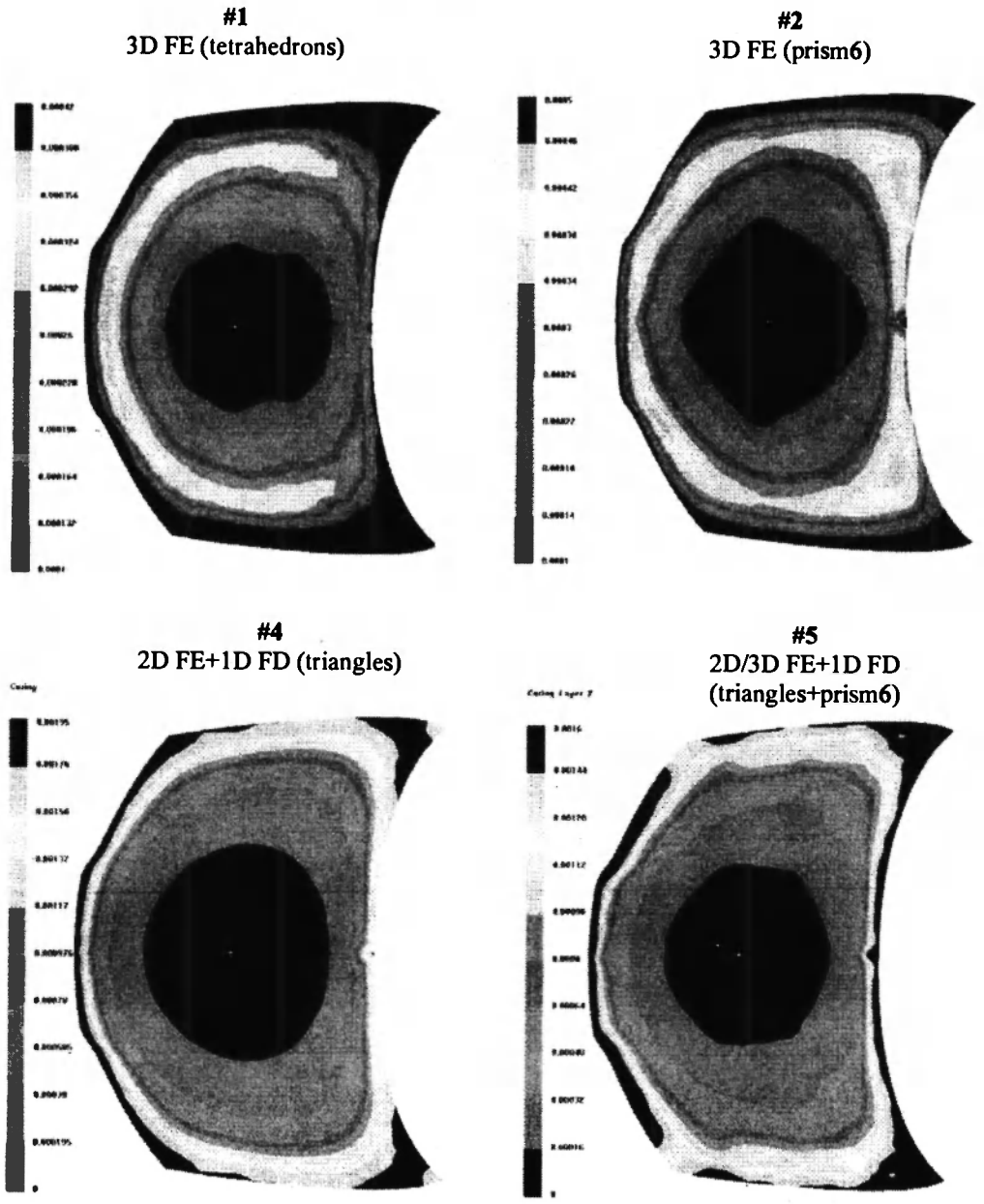

Fig. 24: Degree of conversion at the end of filling in the automotive front hood. The two dimensional solutions seems to better account for cure transport at flow front.

longest residence time and has received the highest amount of heat. As a result of this progressive heating, the maximum degree of polymerization at the end of filling will be found in the latest filled regions and at the periphery of the part. While a degree of cure of about 5e-3 was calculated for the pure 3D formulations (models #1 and #2), a value close to 2e-2 was obtained for the hybrid FE/FD formulations (models #4 and #5). Note that the transport of the degree of cure in the pure 3D solutions shows a diffusion near the flow front. The maximum degree of cure is not exactly at the flow front location as expected. This numerical diffusion is not observed in the hybrid formulations. Table 7 summarizes the results obtained with the five models tested for the filling and curing simulations. The theoretical degree of cure was obtained by solving the

Table 7

Comparison of results obtained with the five models tested for the non-isothermal filling and curing of the automotive front hood.

Model	theoretical	#1	#2	#3	#4	#5
Finite Element	-	tetrahedrons	prism6	triangles	triangles	triangles+prism6
Filling time [sec]	-	450	540.15	502.96	569	589
Cure at end of filling	0.001356	0.00045	0.00047	0.00114	0.00195	0.00167
Mass loss [%]	-	14.6	-0.62	0.12	0.13	-0.63
Total curing time [sec]	1898	2091	1940	1806.3	1903	1845.53
Exothermic temperature [K]	377.35	380	380	375	377	378

kinetic equation at the mold wall temperature (assumed to be the temperature of the resin particles on the flow front near the mold wall). The comparison indicates that 2D heat transport models provide the best predictions of the ultimate degree of polymerization at the end of filling.

Once the mold is filled-up, the simulation continues with a curing analysis until the part is fully cured. Figure 25 shows the degree of resin conversion at 1500 seconds after the beginning of the injection. A curing front from the perimeters of the part towards the centre is induced by thermal effects during filling. Numerical diffusion in the 3D FE formulation still appears as a consequence of the diffused cure transport during filling. Table 7 resumes the curing times and exothermic temperatures for the five models tested. The theoretical values were calculated in a 1D solution for the cavity thickness at the averaged boundary condition between injection resin temperature and initial fibers temperature (considering that injection gate is the latest region to cure). The comparison demonstrates that the 1D FD model in the through-thickness direction is well appropriate to solve this complex thermal problem. Figure 26 compares the computer times required to run each model. While the tetrahedron solution took more than 44 hours, the model with the new *prism6* element required only 1hour 40 minutes, and the hybrid 2D FE/1D FD models around 5 minutes. This study demonstrates the many advantages of the proposed hybrid formulation. The methodology presented here to increase the level of coupling between the physical phenomena that govern the solution is remarkably interesting because of the important savings in time that it brings.

SUMMARY

In this study, a new hybrid finite element/finite difference approximation has been developed to describe the chemorheological behaviors of non-isothermal resin flows and the curing phase in LCM. The fluid flow was computed through the FE/CV method described in /17/, two numerical methods were implemented to solve the energy balance and curing equations. A pure finite element formulation has been initially used to calculate the heat exchanges and resin cure in three-dimensional parts. The method consists of a mixed Galerkin/Lessaint-Raviart schema for heat conduction/diffusion and transport respectively evaluated in a new prismatic *prism6* element. The second approach presented is the hybrid FE/FD scheme. In this case, a finite element formulation used to evaluate the in-plane heat exchange in the part is coupled with a one-dimensional finite difference approximation to calculate the through-thickness heat flow. The latter numerical method is stable and showed much improvement in performance in terms of precision and computational efforts, mainly for large parts.

Comparisons with analytical 2D and 3D heat flows have demonstrated the accuracy of the numerical solutions. Based on the mesh extrusion concept, connected prismatic elements (*prism6*) or non-connected parallel layers of triangles are generated automatically by an extrapolation algorithm from a mid-surface mesh. The combination of the extrusion methodology with the two thermal formulations results in different levels of user defined through-thickness coupling. This allows the selection of increasing levels of complexity to compute the coupled equations.

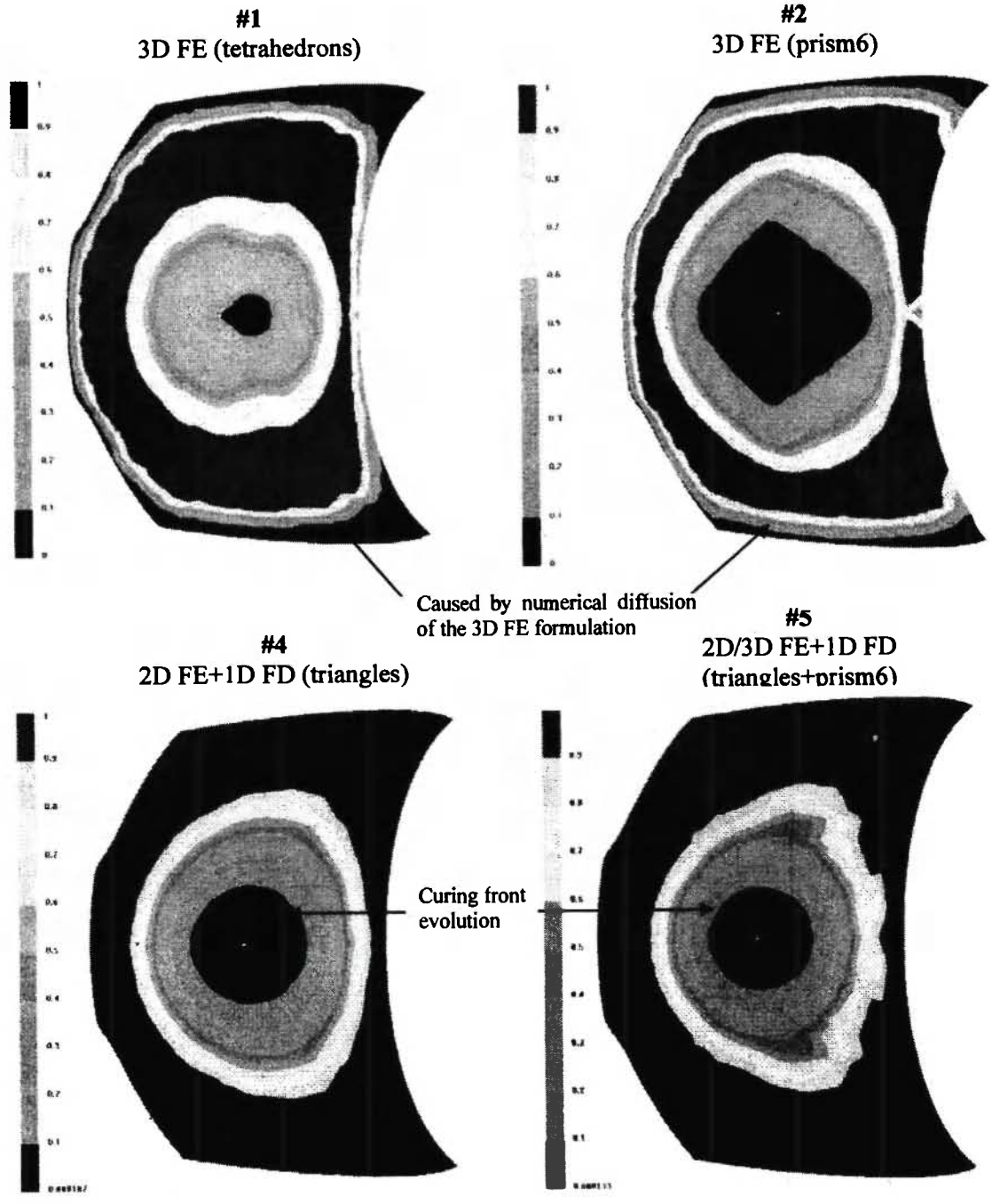

Fig. 25: Evolution of the degree of conversion after filling for a curing time of 1500 sec. A curing front from the part perimeter to the center is induced by the non-isothermal filling.

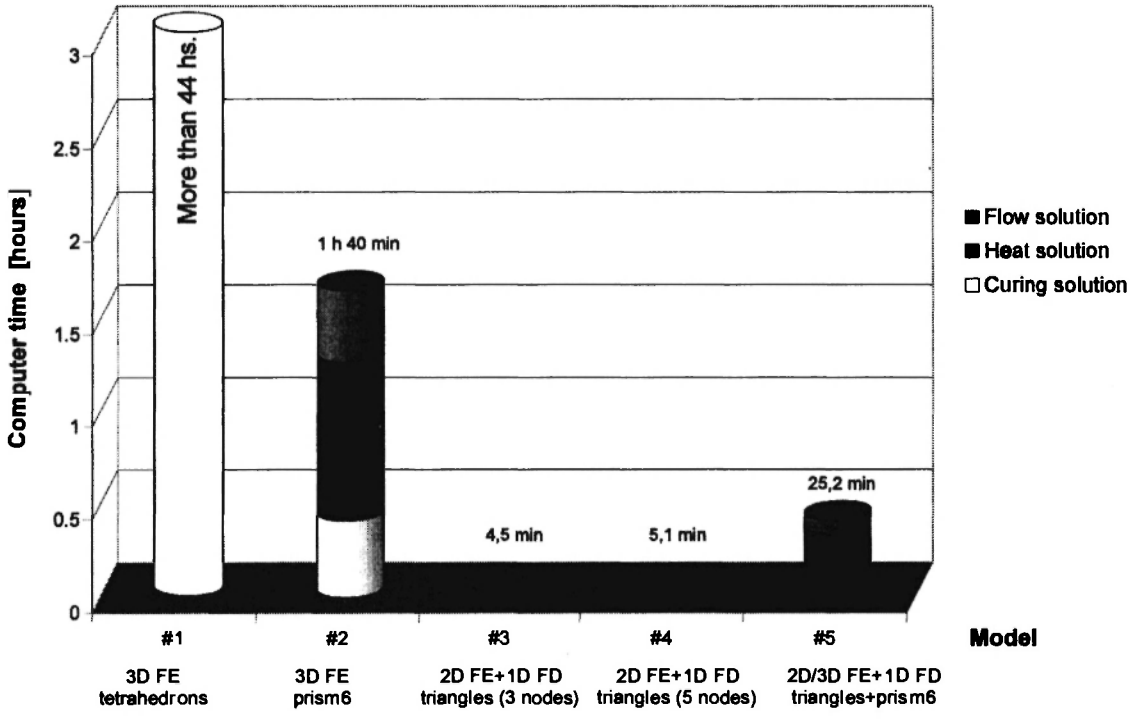

Fig. 26: Comparison of computer times required for each model tested. While previous 3D solutions with tetrahedrons required more than 44 hours, the new *prism6* runs in 1 hour 40 min and the hybrid FE/FD solutions in 5 minutes.

Analysis of a case test was conducted to illustrate the capabilities of the extrusion methodology and of the hybrid FE/FD formulation. A quick evaluation of the virtual process can first be carried out by a simple FE/FD coupling. To obtain more accurate results, the level of coupling can then be progressively increased with the same input mesh and process data. This methodology is promising especially for numerical optimization when a large number of evaluations are required. The optimization algorithm can begin with a simulation model looking for a global optimum and then increase the quality of the model as convergence progresses towards a refined optimum. Future research efforts will aim to implement this possibility.

ACKNOWLEDGEMENTS

The authors thank the *National Science and Engineering Research Council of Canada* (NSERC) and *Fonds Québécois pour la Recherche sur la Nature et la Technologie* (FQRNT) for their financial support. The contribution of *ESI_Group* and their numerical support is also gratefully acknowledged, as well as the program of *Bourses d'Excellence du Ministère de l'Education du Québec* that made this research possible.

REFERENCES

1. Guyonvarch G., Audet M., Qian Y. Y., Trochu F., Delaunay D. Validation of Non-Isothermal Resin Transfer Molding Simulations. *Joint European Conference JEC.* Paris, April 24-26 1996.
2. Lebrun G., Gauvin R. Heat Transfer Analysis in a Heated Mold during the Impregnation Phase of the Resin Transfer Molding Process. *Journal of Material Processing and Manufacturing Sci.* 1995; 4:81-104.
3. Bohr E. *Etude des Échanges Thermiques dans la Fabrication des Composites par les Procédés*

d'Injection sur Renfort. Mémoire de Maîtrise en Sciences Appliquées. Dep. Génie Mecanique. École Polytechnique de Montréal. 2000; 267 pgs.

4. Tucker C. Heat Transfer and Reaction Issues in Liquid Composite Molding. *Polymer Composites* 1996; **17(1)**:60-72.
5. Gauvin R., Trochu F. Key Issues in Numerical Simulation for Liquid Composite Molding Processes. *Polymer Composites*. 1998; **19**:233-240.
6. Ferland P., Trochu F., Gauvin R., Guittard D., Boime B. Rate of Conversion, Temperature Variation and Flow Simulation of Reactive Liquid during RTM and SRIM Mold Filling. *ENERCOMP 95 conf.* Montreal, Quebec, May 1995.
7. Young W.-B. Three-Dimensional Non-Isothermal Mold Filling Simulations in Resin Transfer Molding. *Polymer Composites*. 1994; **15**(2):118-127.
8. Bruschke M. V., Advani S. G. A Numerical Approach to Model Non-Isothermal Viscous Flow Through Fibrous Media with Free Surfaces *International Journal for Numerical Methods in Fluids*. 1994; **19**:575-603.
9. Ngo N. D., Tamma K. K. Non-Isothermal 2D Flow/3D Thermal Developments Encompassing Process Modelling of Composites: Flow/Thermal/Cure Formulations and Validations. *International Journal for Numerical Methods in Engineering*. 2001; **50**:1559-1585.
10. Chang A., Hwang S., Modeling Nonisothermal Impregnation of Fibrous Media with Reactive Polymer Resin. *Polymer Eng. and Sci.* 1992; **32**(5):310-318.
11. Han C., Lem K. Chemorheology of Thermosetting Resins I. The Chemorheology and Curing Kinetics of Unsaturated Polyester Resin. *Journal of Applied Polymer Sci.* 1983; **28**:3155-3183.
12. Castro J .M., Macosko C. W., Perry S. J. *Polymer Commun.* 1984; **25**:82.
13. Lin R. J., Lee L. J., Llou M. L. Mold Filling and Curing Modeling of RTM and SRIM Processes. *Advanced Composite Materials*, Conf. Proceedings, Detroit USA, Sept. 30–Oct. 3 1991; 165-174.
14. Advani S. G. editor, *Flow and Rheology in Polymer Composites Manufacturing*. Elseiver Sci., 1994; ISBN: 0444893474.
15. Rudd C., Long, A., Kendall K., Mangin C. *Liquid Moulding Technologies*. SAE International, 1997; ISBN: 0768000165.
16. Kamal M., Sourour S. Kinetics and Thermal Characterization of Thermoset Cure. *Polymer Eng. Sci.* 1973; **13**(1):59-64.
17. Edu Ruiz, *De la caractérisation des matériaux et simulation du procede à l'optimisation de la fabrication des composites par injection sur renfort.* PhD. Thesis. Dep. Génie Mecanique. Ecole Polytechnique de Montréal. 2004 : 427 pgs.
18. Audet M. *Simulation Numérique Tridimensionnelle du Transfert de Chaleur dans les Moules d'Injection pour Matériaux Composites*. Mémoire de Maîtrise en Sciences Appliquées. Dep. Génie Mecanique. École Polytechnique de Montréal. 1996 ; 305 pgs.
19. Holman J. P. *Heat Transfer*. McGraw Hill, 9th Edition 2002; ISBN: 0072406550.